Published online July 20, 2017

Special Section: The Root Zone: Soil Physics and Beyond

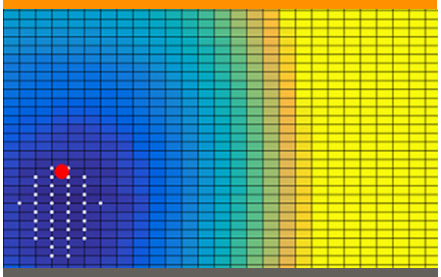

Parameterization of Root Water Uptake Models Considering Dynamic Root Distributions and Water Uptake Compensation

Gaochao Cai,* Jan Vanderborght, Valentin Couvreur, Cho Miltin Mboh, and Harry Vereecken

The spatiotemporal distribution of root water uptake (RWU) depends on the dynamics of the root distribution and compensatory uptake from wetter regions in the root zone. This work aimed to parameterize three RWU models with different representations of compensation: the Feddes–Jarvis model that uses an empirical function, the Feddes model without compensation, and the Couvreur model that is based on a physical description of water flow in the soil–root system. These models were implemented in HYDRUS-1D, and soil hydraulic parameters were optimized by inverse modeling using soil water content and potential measurements and observations of root distributions of winter wheat (*Triticum aestivum* L.) in horizontally installed rhizotubes. Soil moisture was equally well predicted by the three models, and the soil hydraulic parameters optimized by the models with compensation were comparable. The obtained RWU parameters of the Feddes–Jarvis model were consistent with data reported in the literature, although the pressure heads h_{3l} and h_{3h} for lower and higher transpirations rates, respectively, could not be uniquely identified. Response surfaces of the objective function showed that the root-related parameters of the Couvreur model could be identified using inverse modeling. Furthermore, these parameters were consistent with combined root architectural and hydraulic observations from the literature. The Feddes–Jarvis and Couvreur models simulated similar root-system-scale stress functions that link total RWU to the effective root zone water potential, suggesting that parameters may be transferable between the two models. Simulated RWU profiles differed due to different water redistribution by the root system, but the measurements were not sufficiently precise to observe this redistribution.

Core Ideas

- Parameters of different RWU models were optimized using data from a rhizotron facility.
- The same soil hydraulic properties were obtained for models considering RWU compensation.
- Feddes–Jarvis and Couvreur models predicted similar root-system-scale stress functions.
- The obtained RWU parameters were consistent with data reported in the literature.
- The models with compensation predicted similar total uptake but different local RWU.

G. Cai, J. Vanderborght, and H. Vereecken, Agrosphere, Institute of Bio- and Geosciences (IBG-3), Forschungszentrum Jülich GmbH, Jülich, Germany; V. Couvreur, Earth and Life Institute, Univ. catholique de Louvain, Louvain-la-Neuve, Belgium, and Dep. of Land, Air, and Water Resources, Univ. of California, Davis, CA 95616; C.M. Mboh, Institute of Crop Science and Natural Resource Protection, Faculty of Agriculture, Univ. of Bonn, Bonn, Germany. *Corresponding author (g.cai@fz-juelich.de).

Received 8 Dec. 2016.
Accepted 26 Apr. 2017.

Citation: Cai, G., J. Vanderborght, V. Couvreur, C.M. Mboh, and H. Vereecken. 2017. Parameterization of root water uptake models considering dynamic root distributions and water uptake compensation. Vadose Zone J. doi:10.2136/vzj2016.12.0125

Abbreviations: C, Couvreur; ET, evapotranspiration; F, Feddes; FJ, Feddes–Jarvis; GA, genetic algorithm; NRLD, normalized root length density; OF, objective functions; RLD, root length density; RWU, root water uptake; SWC, soil water content; SWP, soil water pressure head.

Numerous root water uptake (RWU) models have been developed with different assumptions, complexity, and parameters, but the description of this process and its parameterization remains challenging in soil hydrology (Kumar et al., 2014; Vereecken et al., 2015). Although it is commonly acknowledged that RWU is defined by water potential gradients and hydraulic resistances in the soil–plant system (Steudle and Peterson, 1998; van den Honert, 1948), this principle is seldom included in models.

Root water uptake models can be divided into two main classes: functional-structural vs. macroscopic models. The former class defines a root system architectural domain facilitating the inclusion of explicit root hydraulic features and associated physical concepts to simulate water flow toward individual roots (Doussan et al., 1998; Javaux et al., 2008). Their complexity is particularly appropriate to address questions of interactions between root growth and soil properties (Pagès et al., 2004; Somma et al., 1998), foraging for soil resources (Lobet et al., 2014; Lynch, 2013; Pagès, 2011), and plant responses

in heterogeneous environments (Couvreur et al., 2014a; Huber et al., 2014).

In macroscopic models, RWU intervenes as a sink term in the soil water flow equation without solving flow toward individual roots. Water uptake is typically assumed to be distributed proportionally to rooting densities and locally adjusted for water availability. The simplicity of this effective approach and the lower computing time are particularly suitable for applications at larger scales (Baram et al., 2016; Feddes et al., 2001; Oleson et al., 2008). However, the parameters and concepts used in these models are to a large extent empirical so that they cannot be linked to directly measurable properties of the root system. Recently, simple one-dimensional macroscopic expressions of RWU were derived based on small-scale hydraulic principles in the soil around roots (de Jong van Lier et al., 2008) and within the root system (Couvreur et al., 2014). This allowed a revision of non-physical assumptions in macroscopic RWU models and linking their parameters to properties of the root system (Javaux et al., 2013).

The parameters of a functional-structural RWU model can be derived from direct measurements (e.g., root architecture, root hydraulic properties). However, these measurements are impractical in the field and hence typically performed in the laboratory on young plants (Doussan et al., 2006; Lobet and Draye, 2013; Steudle et al., 1987) that may not be representative of field conditions. Similarly, soil hydraulic properties can be directly measured or derived from measurements on relatively small soil samples following prescribed experimental protocols. However, soil heterogeneity makes it challenging to get representative properties of larger soil volumes, for instance to describe processes at the field scale (Vereecken et al., 2010, 2015), and hence the interest in simpler approaches that rely on fewer parameters. These parameters are hardly measurable directly but can be fine-tuned so that the models effectively behave like the real system, as commonly done in water management-oriented simulations (Asseng et al., 1998; Deb et al., 2011; Freundl et al., 1998; Hupet et al., 2002). In this context, inverse modeling is adequate to infer soil and root properties from in situ measurements of soil water status (water contents and potentials) and fluxes (Šimůnek and Hopmans, 2009; Vrugt et al., 2001b; Wöhling et al., 2013). With optimization algorithms, inversion approaches search for effective parameter values that optimally reproduce field observations.

The distribution of RWU in the soil profile is greatly affected by the spatial-temporal root distribution. More specifically, RWU is generally assumed to be a direct function of root length densities (RLDs) (Feddes et al., 2001; Heinen, 2014; Molz, 1981). In order to represent the interactions between root development and soil water status, the dynamics of root distributions need to be properly accounted for (Krounbi and Lazarovitch, 2011). However, most simulations of RWU use simplified descriptions to represent root growth and root distributions. Either a logistic or an empirical growth function (Borg and Grimes, 1986; Hoffman and van Genuchten, 1983; Šimůnek and Suarez, 1993) is used to simulate the root development. A few studies have simulated RWU using the measured root distribution obtained from soil cores in lysimeters or in field plots at the end of the crop cycle (Albasha et al., 2015; de Jong van Lier et al., 2008). An important problem with observations of root distributions is that they often require destructive sampling so that the dynamics of root distributions are difficult to observe. Root length density distributions may be estimated from dynamic soil moisture measurements (Hupet et al., 2002, 2003; Musters and Bouten, 1999, 2000; Vrugt et al., 2001a) using inverse modeling. However, these studies also pointed at uncertainties that may arise when the soil hydraulic parameters are not well known. Therefore, direct measurements of RLD distributions and their temporal dynamics are important additional information that can be used to constrain other parameters related to stress and water uptake compensation functions in RWU models. To monitor the evolution of root density profiles noninvasively, the rhizotube or minirhizotron method (Johnson et al., 2001; Rewald and Ephrath, 2012; Smucker et al., 1987; Volkmar, 1993) has been introduced. The observations from minirhizotrons helped to improve the understanding of root dynamics and functions (Garré et al., 2012); however, few studies have used minirhizotron observations to estimate RWU and RWU model parameters (Wu et al., 1999).

The distribution of RWU depends, besides on the root distribution, also on the water availability in the soil profile, which is linked to the soil water potential. When the soil dries out and the water potential decreases and becomes closer to the wilting point, the difference in water potential between the soil and the plant and consequently the RWU decrease. The relation between RWU, soil water potential, and transpiration demand is described by so-called stress functions (Feddes et al., 1978). It should be noted that more precise formulations, which are based on the matric flux potential and account for the difference between the bulk soil water potential and the water potential at the soil–root surface and in the root xylem, have been derived (de Jong van Lier et al., 2008, 2013).

Because the root system is a connected network, this reduction in RWU can be compensated by a higher uptake from wetter soil layers with a higher water potential, i.e., RWU compensation (Huang et al., 1997; Jarvis, 1989; Pang and Letey, 1998; Šimůnek and Hopmans, 2009). Skaggs et al. (2006) reviewed compensatory RWU mechanisms and simulations and suggested that compensation can be of great importance when water potentials vary within the root zone. Actual RWU may be underestimated if compensation is not considered (Kuhlmann et al., 2012). However, the physical basis for the water stress and compensation functions that are currently used in macroscopic models, e.g., the Feddes–Jarvis functions (Feddes et al., 1978; Jarvis, 1989), and that are implemented in the unsaturated zone simulation model HYDRUS-1D

(Šimůnek et al., 2013), can be debated, e.g., Javaux et al. (2013). For instance, the compensation term was defined in terms of the local water stress function, whereas compensation represents the non-local nature of RWU, i.e., RWU at one location also depends on the water potential at other locations and compensation may occur independently of water stress. Alternatively, physically based macroscopic stress and compensation functions can be derived from an analysis and upscaling of functional-structural soil–root architecture models (Couvreur et al., 2012, 2014; Javaux et al., 2013). Studies that tested and parameterized these different stress and compensation functions using field measurements are, however, scarce (Dong et al., 2010; Li et al., 2001) and have not yet been performed for the physically based macroscopic model.

In this study, we focused on the Feddes–Jarvis (Šimůnek and Hopmans, 2009) (FJ) and the Feddes (Feddes et al., 1978) (F) models, which are often used for RWU simulations, and the physically based macroscopic Couvreur et al. (2012) model (C). The objectives of this study were (i) to parameterize the soil hydraulic properties, water stress, and compensation functions of the three models from time series of soil water status that were measured at six depths under growing winter wheat and using data of root distributions obtained from rhizotubes; and (ii) to compare the transpiration fluxes and RWU profiles that are predicted by the calibrated models. We tested whether the time series of water status can be described equally well by the different models and whether differences in RWU models can be compensated by a different parameterization of the soil hydraulic properties. We hypothesized that the inversely estimated parameters are consistent with literature data (the FJ model) and with parameters that are directly derived from a root architecture model (the C model).

Theory

Spatial-temporal distributions of the water content in the soil are obtained from numerical solutions of the Richards equation, which describes the water fluxes in the water balance equation using the Buckingham–Darcy equation and uses a sink term to represent RWU:

$$\frac{\partial \theta}{\partial t} = \frac{\partial}{\partial z}\left[K(h)\left(\frac{\partial h}{\partial z}+1\right)\right] - S(z,t) \quad [1]$$

where θ represents the volumetric soil water content (SWC) [L^3 L^{-3}], t is time [T], z is the elevation [L], h is the soil water pressure head (SWP) [L], K is the hydraulic conductivity function [L T^{-1}], and S is the sink term [L^3 L^{-3} T^{-1}], defined as the volume of water removed from a unit volume of soil per unit time due to root extraction.

According to the van Genuchten–Mualem constitutive model (Mualem, 1976; van Genuchten, 1980), the soil water retention and soil hydraulic conductivity functions are given by

$$\theta(h) = \begin{cases} \theta_r + \dfrac{\theta_s - \theta_r}{\left[1+|\alpha h|^n\right]^m} & h<0 \\ \theta_s & h\geq 0 \end{cases} \quad [2]$$

$$K(S_e) = K_s S_e^l \left[1-\left(1-S_e^{1/m}\right)^m\right]^2 \quad [3]$$

where θ_r and θ_s are the residual and saturated water contents [L^3 L^{-3}], respectively, S_e is the relative saturation: $S_e = (\theta - \theta_r)/(\theta_s - \theta_r)$ (dimensionless), and K_s is the saturated hydraulic conductivity [L T^{-1}]. The parameters α (L^{-1}), n, m ($m = 1 - 1/n$, $n > 1$), and l are empirical coefficients affecting the shape of the hydraulic functions.

Feddes and Feddes–Jarvis Models

In the RWU model defined by Feddes et al. (1978), the sink term is a function of potential transpiration, the vertical root distribution, and the pressure head and is expressed as

$$S_F(z) = \alpha_F(h) T_{pot} \mathrm{NRLD}(z) \quad [4]$$

$$\alpha_F(h) = \begin{cases} 0 & h\geq h_1,\ h\leq h_4 \\ \dfrac{h-h_1}{h_2-h_1} & h_2 \leq h < h_1 \\ 1 & h_3 < h \leq h_2 \\ \dfrac{h-h_4}{h_3-h_4} & h_4 < h \leq h_3 \end{cases} \quad [5]$$

$$T_{pot} = \mathrm{ET}_{pot}\left[1-\exp(-k\mathrm{LAI})\right] \quad [6]$$

$$\mathrm{NRLD}(z) = \frac{\mathrm{RLD}(z)}{\int_0^{l_z} \mathrm{RLD}(z)\,dz} \quad [7]$$

where $\alpha_F(h)$ is the water stress response function ($0 < \alpha_F < 1$) (dimensionless); h_1 and h_4 are the anaerobiosis and the wilting point above and below which RWU is null, respectively; h_2 and h_3 are the pressure heads between which RWU keeps the maximum rate; T_{pot} is potential transpiration [L T^{-1}]; ET_{pot} is potential evapotranspiration [L T^{-1}]; k is a constant representing the extinction coefficient per unit leaf area (0.6 was used in this study) (Allen et al., 1998; De Faria et al., 1994; Mo and Liu, 2001); LAI is the leaf area index; NRLD is normalized root length density [L^{-1}]; RLD is root length density [L L^{-3}], and l_z is the rooting depth [L]. Note that α_F depends also on T_{pot} because the critical point (h_3) is a piecewise linear function of T_{pot} (Šimůnek et al., 2013; Wesseling and Brandyk, 1985):

$$h_3 = \begin{cases} h_{3h} & T_{pot} > T_{3h} \\ h_{3h} + \dfrac{(h_{3l}-h_{3h})(T_{3h}-T_{pot})}{(T_{3h}-T_{3l})} & T_{3l} < T_{pot} < T_{3h} \\ h_{3l} & T_{pot} < T_{3l} \end{cases} \quad [8]$$

where h_3 is smaller (h_{3l}, more negative) for lower potential transpiration rates (T_{3l}) and higher (h_{3h}) for higher transpiration rates (T_{3h}). The dependency of h_3 on T_{pot} can be considered to effectively represent the greater pressure drop in the plant from the root system to the shoot under higher than under lower transpiration rates. Assuming that the pressure head in the shoots regulates stomatal closure and the stomatal closure will be triggered for higher SWPs when the transpiration rate is higher.

The stress function α_F, which reduces the water uptake at a certain depth, is a local function that depends only on the pressure head at that depth. However, because the root system is a connected network, RWU at a certain depth is influenced by pressure heads and uptake at other depths. To account for these non-local effects, a plant water stress index ω was introduced in the FJ model, which integrates the stress function over the root zone using the normalized root density function as a weighting function (Jarvis, 1989; Šimůnek and Hopmans, 2009):

$$\omega = \int_{l_z} \alpha_F(h)\mathrm{NRLD}(z)\mathrm{d}z \quad [9]$$

It is assumed that as long as this plant stress index is above a certain threshold value, ω_c, the total RWU is equal to the T_{pot} and decreases linearly with decreasing ω when ω is below ω_c:

$$\frac{T_{act}}{T_{pot}} = \begin{cases} 1 & \omega_c < \omega \leq 1 \\ \dfrac{\omega}{\omega_c} & \omega < \omega_c \end{cases} \quad [10]$$

where T_{act} is the actual RWU [L T^{-1}]. Therefore, RWU at a certain depth in the model is obtained by combining Eq. [4] and [10]:

$$S_{FJ}(z) = \alpha_F(h)\mathrm{NRLD}(z)T_{pot}\frac{1}{\max(\omega,\ \omega_c)} \quad [11]$$

The parameter ω_c controls the ability of the plant to compensate for reduced water uptake at a certain depth by increasing water uptake in the root profile. For $\omega_c < 1$, water uptake is, in fact, increased at all depths compared with the case when no uptake compensation is considered, which corresponds to $\omega_c = 1$. However, the increase is larger in the wetter parts of the root zone where $\alpha_F(h)$ is larger.

Couvreur Model

A new three-dimensional macroscopic RWU model based on root system hydraulic architecture and the analytical solution of the flow equation in the root network was developed by Couvreur et al. (2012), in which parameters were not defined at the root segment scale but at the soil element or the plant scale. For densely sown crops such as wheat, the three-dimensional high-resolution model can be upscaled to a one-dimensional model (Couvreur et al., 2014). The one-dimensional model describes gradient-based water flow in the coupled soil–root architecture considering the hydraulic conductance of the soil–root system:

$$S_C(z) = K_{rs}(h_{Te} - h_{Tleaf})\mathrm{NRLD}(z) + K_{comp}[h_T(z) - h_{Te}]\mathrm{NRLD}(z) \quad [12]$$

where

$$\begin{cases} K_{rs}(h_{Te} - h_{Tleaf}) = T_{pot} & \text{when } h_{Tleaf} > h_{Tleaf\_crit} \\ K_{rs}(h_{Te} - h_{Tleaf\_crit}) = T_{act} & \text{else} \end{cases} \quad [13]$$

$$h_{Te} = \int_0^{l_z} h_T(z)\mathrm{NRLD}(z)\mathrm{d}z \quad [14]$$

where K_{rs} is the one-dimensional equivalent conductance of the root system [T^{-1}], K_{comp} is the compensatory RWU conductance of the plant [T^{-1}], h_T is the total soil hydraulic head (pressure head plus elevation head: $h + z$) [L], h_{Te} is the effective root zone hydraulic head sensed by the plant [L], and h_{Tleaf} is the leaf water hydraulic head [L], which can be obtained from Eq. [13]: $h_{Tleaf} = h_{Te} - T_{pot}/K_{rs}$; h_{Tleaf_crit} is a critical leaf hydraulic head that is constant by stomatal regulation in isohydric plants (Tardieu and Simonneau, 1998).

According to Eq. [12], RWU is split into two components: an uptake component that corresponds to the uptake from a profile in hydrostatic equilibrium with a homogeneous hydraulic head and a compensatory component that describes the increase or decrease of local water uptake due to a locally higher or lower hydraulic head than the effective hydraulic head h_{Te}. In contrast to the original models of Couvreur et al. (2012), we used a NRLD function to describe the RWU in a soil profile with uniform hydraulic head and to weight the local h_T for the calculation of h_{Te}. Couvreur et al. (2012, 2014) demonstrated that the weighting function used in Eq. [12] and [14] might deviate from NRLD depending on the hydraulic parameters (radial conductivity, axial conductance, etc.) of the root segments.

Materials and Methods

Measurements

Root distributions, SWC, and soil water potential were measured in a cropped field in Selhausen (50°52′ N, 6°27′ E), Germany. The field is slightly inclined, with a slope <4°, and the soil is characterized by a strong gradient in soil texture, with 60% gravel content at the upper slope and 4% in the footslope, respectively (Vanderborght et al., 2010). At the site, two minirhizotron facilities were constructed, one at the upper and one at the lower site of the field. In each facility, three 7- by 3-m plots—a rain sheltered, a rainfed, and an irrigated plot—were established. The construction of the facilities and the technical details of the instrumentation were described by Cai et al. (2016). Because the objective of this

study was to compare the performance of different RWU models and to evaluate a procedure to determine their parameters by inverse modeling, we focus here on data from the sheltered plot in the upper facility with the stony soil. In the future, we will evaluate the effect of the treatments and the soil types on root development and the parameters of RWU models. Winter wheat was sown with a seed density of 300 to 320 grains m^{-2} on 31 Oct. 2013 and harvested on 17 July 2014. The fertilizer rate of 120 kg N ha^{-1} (KAS 27) was applied on 21 March, and 60 kg N ha^{-1}, 30 kg P ha^{-1} (as P_2O_5), and 116 kg K ha^{-1} (as K_2O) were applied on 6 May 2014. After completion of stem extension, the plots were covered at four times during rainy periods (6–15 May, 21–23 May, 25–28 May, and 4–15 July) and approximately 197.2 mm of rainfall was sheltered out. One irrigation event with 14.7 mm was applied on 9 June 2014.

Soil water content and soil water potential were monitored hourly by homemade time domain reflectometer (TDR) probes (Cai et al., 2016; Weihermüller et al., 2013), tensiometers (T4e, UMS GmbH), and dielectric water potential sensors (MPS-2 matrix water potential and temperature sensor, Decagon Devices), respectively. The sensors were installed at the 10-, 20-, 40-, 60-, 80-, and 120-cm depths. Soil water content is presented as the mean of the data that were monitored by the four TDR sensors at each depth. Root development was observed in 7-m-long rhizotubes (clear acrylic glass tubes with outer and inner diameters of 64 and 56 mm, respectively) of which three replicates were horizontally installed at the same depths as the SWC sensors. Soil water potential was converted to SWP in the later simulation. There was a horizontal offset of 0.1 m between rhizotubes at different depth levels to make sure that rhizotubes at a certain depth were not overlain by rhizotubes at other depths. Root measurements were performed repeatedly from both left and right sides of the rhizotubes at 20 locations along each tube by a digital camera (Bartz Technology Corporation). The images with a size of 13.5 by 18 mm were analyzed with Rootfly (Wells and Birchfield, 2009).

Generally, RLD is expressed as root length per unit volume of soil (L L^{-3}), but in rhizotubes the number of roots or the root length in an observation window is observed. This corresponds with a root length per surface or root number per surface. These observations can be translated into a root length per volume by multiplying the root length per surface with a soil depth factor that represents the "observation depth" from the tube surface. Upchurch (1987) indicated that the observed soil depth from the tube surface ranged from 1 to 3 mm according to the soil texture. Steele et al. (1997) used 2 mm for coarse sand soil, and Garré et al. (2011) used 1 mm for loamy sand. However, this depth of view from the tube is arbitrary. Machado et al. (2003) used root intensity instead, being root length per unit area (L L^{-2}) that was observed from rhizotubes. However, a problem with root length observations around rhizotubes is that root growth may be affected by disturbances at the rhizotube surface and therefore not representative of root length densities in the bulk soil. Therefore, Garré et al. (2012) used root impacts (total primary root counts per observed area) on the rhizotubes. The relation between root impacts and RLD depends on the geometry of the root system (Vansteenkiste et al., 2014) but is not influenced so strongly by the presence of the rhizotubes. To relate the impacts to RLD, we assumed that RLD and impact are proportional and that the proportionality factor does not depend on the observation depth, which is an approximation. The proportionality factor cancels out when calculating the NRLD so that it does not need to be defined.

Root measurements were performed 22 times weekly from 11 Feb. (tillering period) to 14 July 2014 (ripening period). Weekly measurements were frequent enough to capture the behavior of root development (Vamerali et al., 2012). Figure 1 shows the distribution of the NLRDs. At the beginning of the observation, roots reached the tubes at 40 cm and the RLD decreased with increased soil depths. The NRLD decreased at shallow depths (e.g., 10 and 20 cm) and increased at deeper depths (e.g., 40 cm) as roots developed. It must be noted that the decrease in NRLD in the upper soil layers (10–20-cm depth) was not only due to an increase in root density in lower layers but also due to root decay.

Leaf area index was measured by a plant canopy analyzer (LAI-2200, LI-COR Inc.) (Fig. 2). The meteorological data, e.g., global and net radiation, precipitation, air temperature, wind speed, and relative humidity, were monitored at 2 m above the soil level at 10-min intervals in a mini-weather station that was 140 m away from the test site. During the experimental period from 11 Feb.

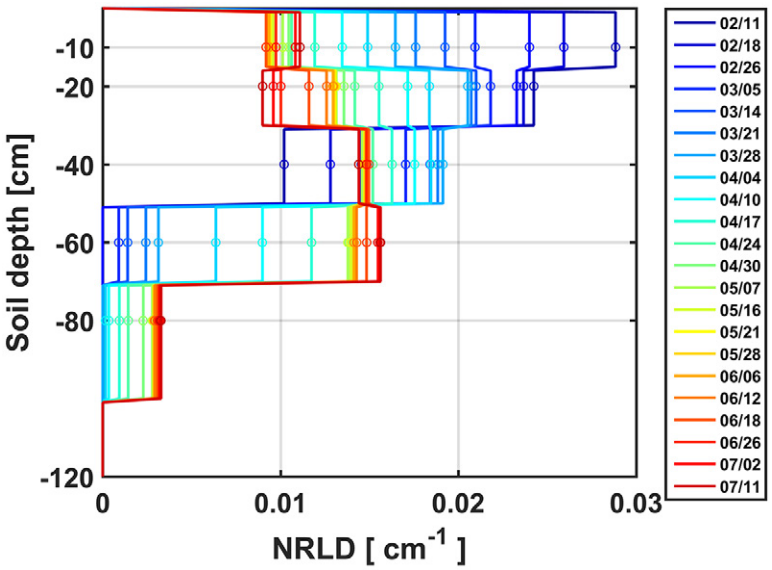

Fig. 1. Spatial and temporal distribution of normalized root length density (NRLD) along the soil profile for 22 weekly measurements. The circles are the measurement locations.

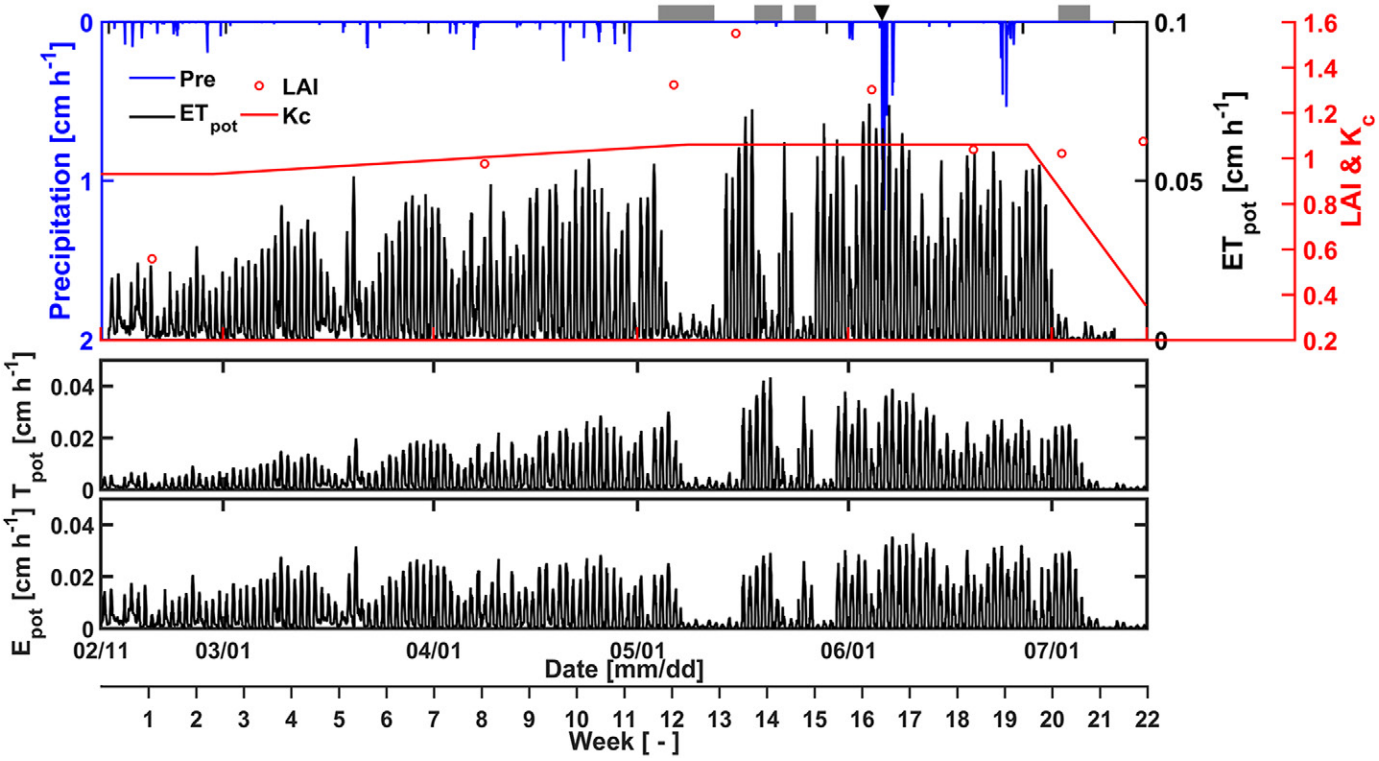

Fig. 2. Variations in precipitation (blue), potential evapotranspiration (ET_{pot}; black), leaf area index (LAI; red dots), and crop coefficient (K_c; red line), along with potential transpiration (T_{pot}) and potential evaporation (E_{pot}) separately. Sheltered periods (■) and irrigation (▼, 14.7 mm) are indicated across the top.

to 14 July 2014, the amount of precipitation was 312.6 mm. The potential crop evapotranspiration was obtained using the Penman–Monteith equation (Allen et al., 1998):

$$ET_{pot} = K_c ET_o \quad [15]$$

where ET_o is the reference evapotranspiration [L T^{-1}] and K_c is the crop coefficient (dimensionless). The K_c values for the different plant development stages with corrections for wind speed, the minimum daily relative humidity, and the crop height were obtained from Allen et al. (1998). The potential transpiration and potential evaporation (E_{pot}) were separated by Eq. [6] and [15], and the hourly variations during the measurement period are shown in Fig. 2.

Model Setup and Simulation Runs

For the numerical simulations, we considered a 145-cm-deep soil profile, which was discretized into 1-cm-thick intervals. Two soil layers with different soil hydraulic parameters were considered: 0 to 30 cm (the tillage layer) and 30 to 145 cm. The parameters of the water retention curve, θ_r, θ_s, α, and n, were obtained from fitting Eq. [2] to the observed SWC and SWP in the two soil layers and are listed in Table 1 (see Cai et al., 2016).

Other parameters (e.g., K_s, l) were obtained by inverse modeling. Therefore, the HYDRUS model (Vereecken et al., 2016) was used to solve the Richards equation and simulate the water potentials and water contents that were compared with measured values to derive the parameters in the three models. An atmospheric boundary with surface layer and free drainage were used as the upper and lower boundary conditions, respectively. For the upper boundary, the parameter hCritA, which defines the minimum pressure head that can be reached at the soil surface, was estimated using inverse modeling. The value of hCritA could be obtained from the air humidity (Feddes et al., 1974), but this would lead to values much lower than the permanent wilting point. It has been suggested that hCritA ranges from −150 to −1000 m for different soil textures (Šimůnek et al., 2013). For evaporation from a soil surface on which a crop is growing, the resistance to vapor transfer from the soil surface into the air also contributes to the reduction of evaporation, which is not considered in the splitting of evapotranspiration into evaporation and transpiration (Eq. [6]). Therefore, we considered optimizing hCritA in the simulations.

Table 1. Hydraulic parameters of the Mualem–van Genuchten functions: residual soil water content θ_r, saturated soil water content θ_s, and curve fitting parameters α and n.

Depth	θ_r	θ_s	α	n
cm	——— $cm^3\ cm^{-3}$ ———		cm^{-1}	
0–30	0.0430	0.3256	0.0361	1.3860
30–120	0.0534	0.2286	0.0495	1.5340

The parameters K_s and l of the two soil layers were obtained using inverse modeling. To avoid the physically unrealistic behavior with $dK/d\theta < 0$, we constrained the lower boundary for l by the criterion given by Lambot et al. (2002):

$$l > -2\frac{\left(1-S_e^{1/m}\right)^{m-1}S_e^{1/m}}{1-\left(1-S_e^{1/m}\right)^{m}} \quad [16]$$

For the RWU parameters, the following parameters were kept fixed: $h_1 = 0$, $h_2 = -1$ cm, $h_4 = -16{,}000$ cm (Wesseling, 1991), $h_{Tleaf\_crit} = -16{,}000$ cm (we set $z = 0$ at the soil surface and defined the critical collar hydraulic head). We decided not to fit h_{Tleaf_crit}, T_{3h}, and T_{3l} because these parameters are generally assumed not to vary among different crops (Kropff and van Laar, 1993; Nelsen et al., 1978; O'Toole and Moya, 1981; Shimshi, 1979); T_{3h} and T_{3l} were set to 0.02 and 0.004 cm h^{-1}, respectively (Groh et al., 2016; Yang et al., 2009).

We considered three different inverse modeling setups: Case 1, the FJ model with inverse estimation of ω_c, h_{3h}, and h_{3l}; Case 2: the F model (no compensation, $\omega_c = 1$) with inverse estimation of h_{3h} and h_{3l}. For the C model, Case 3, K_{rs} and K_{comp} were optimized. However, K_{rs} and K_{comp} depend on the root architecture and increase when the root system grows (Doussan et al., 2006; Pierret et al., 2006). We assumed that K_{rs} and K_{comp} were proportional to the total root length so that their values at the ith week could be calculated from the initial K_{rs_ini} or K_{comp_ini} and the integrated root lengths (IRLs) at the ith week and at the start of the observations:

$$K_{rs,i} = K_{rs\_ini}\frac{IRL_i}{IRL_{ini}} \quad [17]$$

where IRL is

$$IRL = \int_{l_z} RLD(z)dz \quad [18]$$

We optimized K_{rs_ini} and K_{comp_ini} of the first week.

The simulations were run with hourly boundary conditions for 154 d from 11 Feb. to 14 July 2014. As initial conditions, the pressure heads measured at the start of the simulation period were used. We assumed that the root distribution in every soil layer was constant for 7 d. Because only one root distribution can be used as input in HYDRUS-1D, 22 input files (each covering a time span of 1 wk) were created for 22 successive HYDRUS-1D simulations. The simulated SWP profile at the end of each week was used as the initial condition for the simulation of the next week.

The procedure of the inverse modeling and simulations is depicted in Fig. 3. Before performing the simulations of RWU, candidate values for two soil hydraulic parameters $K_{s(1,2)}$ and $l_{(1,2)}$ of the top- and subsoil, h_{3h}, h_{3l}, ω_c, K_{rs_ini}, and K_{comp_ini} were sampled by the optimizer (described below) at the beginning of the first week. The simulations were performed separately in HYDRUS for the FJ, F, and C models. Note that executable HYDRUS files for the FJ, F, and C models are different (a modified HYDRUS-1D contains the C model). For each newly started simulation, new candidate parameters $K_{s(1,2)}$, $l_{(1,2)}$, ω_c, h_{3h}, h_{3l}, K_{rs}, and K_{comp} were sampled from uniform distributions with the boundaries given in Table 2.

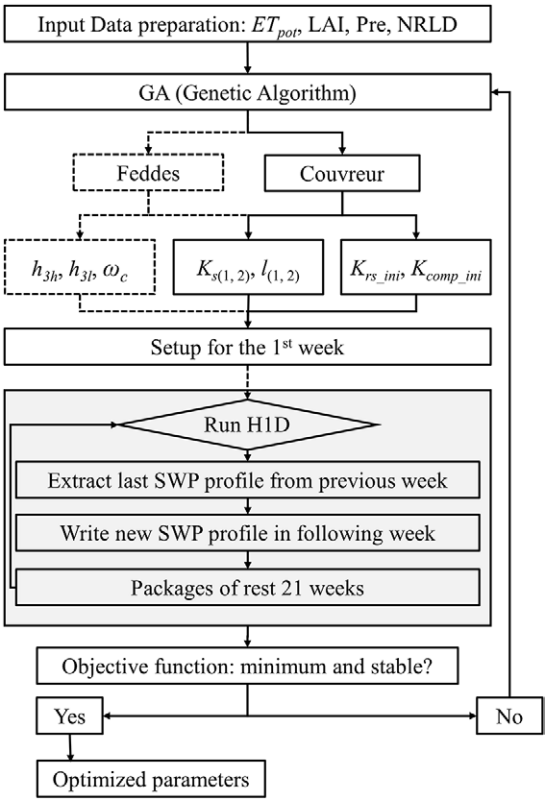

Fig. 3. Procedure for optimization of soil hydraulic parameters by the Feddes–Jarvis or Feddes (dashed lines) model and K_{rs}, K_{comp} by the Couvreur model (solid lines) in the Hydrus-1D (H1D) framework and sequential simulations of root water uptake (RWU) with observed dynamic root distributions, where ET_{pot} is potential evapotranspiration; LAI is leaf area index; Pre is precipitation; NRLD is normalized root length density; h_{3h} and h_{3l} are water potential at high and low transpiration, respectively; ω_c is the critical water stress threshold; K_s is saturated conductivity; l is an empirical model parameter; 1 and 2 are top- and subsoil, respectively; K_{rs_ini} is equivalent conductance of the root system in the first week; K_{comp_ini} is compensatory RWU conductance of the roots in the first week; and SWP is soil water pressure head.

In the inverse modeling steps, the optimum parameters were obtained by systematically minimizing the deviations between the observed (Obs) and simulated (Sim) variables. The considered variables were: SWC, difference in SWC during a time period (dSWC); SWP, difference in SWP during a time period (dSWP); Sto, water storage (integration of SWC from 0–125 cm); dSto, difference in water storage between each time and the first time;

Table 2. Boundaries of the soil hydraulic parameters saturated hydraulic conductivity ($K_{s1,2}$) and empirical coefficient ($l_{1,2}$) in the top- and subsoil, minimum pressure head at the soil surface (hCritA), pressure heads at high (h_{3h}) and low (h_{3l}) transpiration rates, and critical water stress threshold ω_c in the Feddes and Feddes–Jarvis models, and root system (K_{rs}) or compensatory (K_{comp}) root water uptake conductance in the Couvreur model.

Parameter†	Lower bound	Upper bound
$\log_{10}(K_{s1,2})$, cm h^{-1}	−1.8802	0.9198
$l_{1,2}$	−4.000	6.000
$\log_{10}(\lvert hCritA\rvert)$, cm	2	4.5
h_{3h}, cm	−700	−200
h_{3l}, cm	−1500	−600
ω_c	0	1
$\log_{10}K_{rs}$, h^{-1}	−6.480	−4.880
$\log_{10}K_{comp}$, h^{-1}	−7.880	−5.380

† The $\log_{10}$–transformed values were transformed back to the normal form in the subsequent inverse modeling and simulations.

cumT (cumT$_{pot}$: Obs, cumT$_{act}$: Sim; note that T_{act} is the actual RWU). To avoid the impact of noise on the variables that represent changes with time, differences between observations (dSWC and dSWP) were calculated for 4, 10, and 25 d to represent the short, medium, and longer term changes. The deviations between measured and simulated values were evaluated using the following objective function (OF) that aggregates normalized root mean squared errors of the different considered variables (Baram et al., 2016):

$$\mathrm{OF}=\sum_{j=1}^{J}\frac{\sqrt{\sum_{i=1}^{N_j}\left(\mathrm{Sim}_{i,j}-\mathrm{Obs}_{i,j}\right)^2 w_{i,j}}}{\overline{\mathrm{obs}_{i,j}}}\,p_j \qquad [19]$$

where j refers to the number of variables and i to the number of the measurement in the data set of variable j that contains N_j measurements. The weights w were defined as

$$w_{i,j}=\begin{cases}\dfrac{1}{N_j} & \text{variable}\left(\mathrm{SWC},\ \mathrm{SWP},\ \mathrm{Sto},\ \mathrm{cumT}\right)\\ \dfrac{\left|\mathrm{Sim}_{i,j}\right|+\left|\mathrm{Obs}_{i,j}\right|}{\sum_{i=1}^{N_j}\left(\left|\mathrm{Sim}_{i,j}\right|+\left|\mathrm{Obs}_{i,j}\right|\right)} & \text{changes of the variable}\left(\mathrm{dSWC},\ \mathrm{dSWP},\ \mathrm{dSto}\right)\end{cases} \qquad [20]$$

For the variables SWC, SWP, Sto, and cumT, equal weight was given to each measurement, whereas dSWC, dSWP, and dSto were weighted proportionally to the amplitude of the variables so that large variations (e.g., a jump in SWC after a precipitation event) were attributed more weight. In contrast, small fluctuations (e.g., scattering in monitoring) contributed less to the OF. For instance, when neither measurements nor simulations fluctuated at a particular depth, extra weight was attributed to other depths and times to focus on the most informative parts of the signal (Baram et al., 2016). The weighted root mean square errors of each variable were normalized by the mean absolute values of the corresponding variable, $\overline{\mathrm{Obs}}$, to factor out the impact of the different dimensions of the terms in the aggregated objective function. The weights of the different variables in the aggregated objective function (p) were chosen somewhat arbitrarily as: SWC, 10%; dSWC, 10%; SWP, 30%; dSWP, 15%; Sto, 15%; dSto, 15%; and cumT, 5%. The total weight attributed to soil moisture measurements (50%) was partitioned between local (SWC and dSWC) and integrated observations (Sto and dSto). While the former aim at minimizing absolute differences in individual layers, they do not suffice to minimize absolute deviations from the overall soil water balance, which is the role of the latter variables in the OF. The variable cumT was included in the OF with a minor weight to limit deviations between potential and actual cumulative transpiration. This was necessary to avoid undesired drift of the optimizer toward parameter sets predicting extreme water stress events during the whole simulation period (even at springtime when rainfall was abundant).

To minimize the OF, the forward simulations were combined with a genetic algorithm (GA) from the global optimization toolbox of MATLAB 2015b (main functions: ga, gaoptimset) (MathWorks, 2015), with 100 parameter sets as the initial population. To test the matches between the measured and predicted parameters for the three models, the comparisons were evaluated by root mean square error (RMSE), the mean bias error (ME) (Shen et al., 1998), and an index of agreement (d, dimensionless) (Willmott et al., 1985):

$$\mathrm{RMSE}=\sqrt{\frac{\sum_{i=1}^{N}\left(\mathrm{Sim}_i-\mathrm{Obs}_i\right)^2}{N}} \qquad [21]$$

$$\mathrm{ME}=\frac{\sum_{i=1}^{n}\left(\mathrm{Sim}_i-\mathrm{Obs}_i\right)}{N} \qquad [22]$$

$$d=1-\frac{\sum_{i=1}^{N}\left(\mathrm{Sim}_i-\mathrm{Obs}_i\right)^2}{\sum_{i=1}^{N}\left(\left|\mathrm{Sim}_i-\overline{\mathrm{Obs}}\right|+\left|\mathrm{Obs}_i-\overline{\mathrm{Obs}}\right|\right)^2} \qquad [23]$$

To evaluate the uniqueness of the inversely estimated parameters, Bayesian statistics can be used to derive posterior probability distributions of the optimized parameters (Vrugt and Ter Braak, 2011). However, because of computational limitations, we were not able to apply these methods. To get an appraisal of the confinement of the parameters, response surfaces of the OF (Eq. [19]) were generated using possible combinations of two selected parameters while keeping the other parameters at their optimized values (Šimůnek et al., 1998; Toorman et al., 1992). The response surfaces illustrate the sensitivity and the correlations between parameters and whether the estimated values are in a local or global minimum. The range of each parameter was subdivided into 50 intervals so

that response surfaces were constructed from a grid of values with 2500 grid points.

Scenarios Investigated

To evaluate the effect of RWU compensation on the simulated transpiration, we considered a scenario in which parameters were the same as the optimized parameters of the FJ model but with $\omega_c = 1$. The difference between this scenario (F_{w1}) and the simulations with the optimized FJ model better represents the effect of RWU compensation than the difference between the optimized FJ and F models. Root water uptake compensation could be partly accounted for in the F model by adapting stress and soil hydraulic parameters.

The soil at the test site is quite stony and has a low water holding capacity (see the low θ_s in Table 1, especially in the subsoil). The saturated conductivity K_s of such a soil depends strongly on the stone content (Novák et al., 2011). To evaluate the effect of K_s on the simulated transpiration, we performed a second sensitivity analysis. The transpiration was simulated using optimized root parameters of the different water uptake compensation models for a range of K_s values obtained from the literature and representing soil textures from sandy loam to silty clay (Carsel and Parrish, 1988).

Results and Discussion

Simulation of Soil Moisture and Water Fluxes Using Optimized Parameters

The time courses of observed and simulated SWC and SWP that were simulated by the FJ model with compensation, F and F_{w1} models without compensation, and by the C model using the optimized parameters are depicted in Fig. 4 at six soil depths and at a daily time scale for the observation period. Using the time series of measured root distributions, SWCs and SWPs simulated by both models responded well to hydrologic changes: gradual decreases during dry spells and rapid increases due to precipitation and irrigation events. However, discrepancies also exist. The absolute values of SWPs at 10 cm from mid-April to mid-May and at 80 cm during June were underestimated. The SWC in the topsoil and the SWP in the whole soil profile were not well described after the last rain event (on the right side of the vertical dashed line in Fig. 4) when the shelter was partly uncovered because of a thunderstorm, probably causing an offset between measured and actual infiltration rates. In the inverse modeling, this part was thus not considered (the vertical dashed line marks the end of the optimization period). Visually, there was no obvious difference between the simulations that were modeled by the FJ, F, F_{w1}, and C models. The different models also simulated similar differences for dSWC and dSWP (see, for instance, dSWC and dSWP during a 4-d period in Supplemental Fig. S1).

The cumulative RWU and the water flux that were simulated by the FJ, F, F_{w1}, and C models with the optimized soil hydraulic

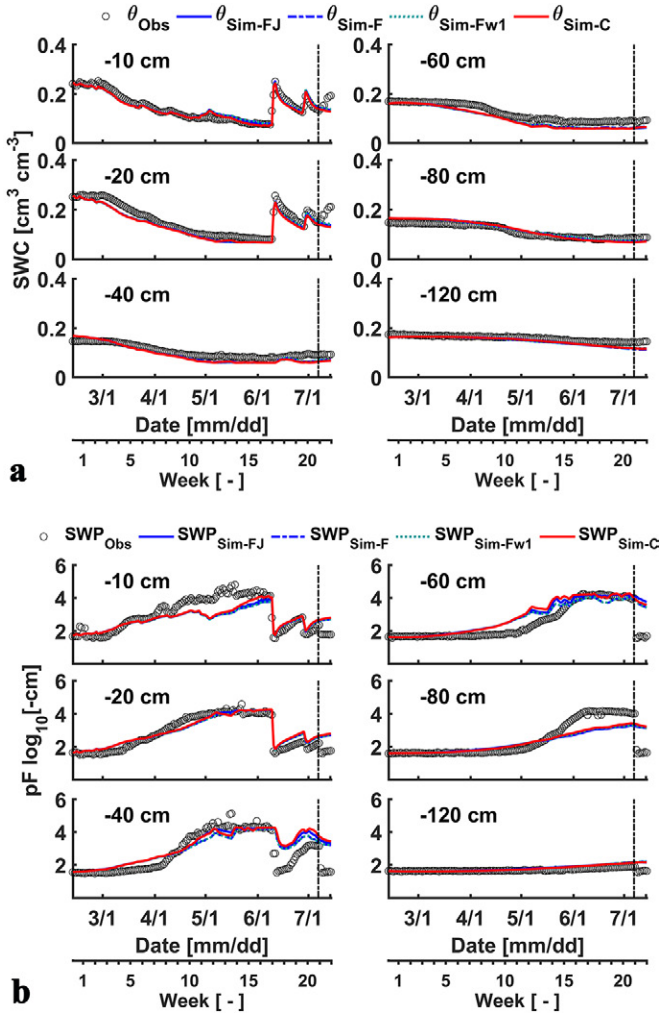

Fig. 4. Comparison of (a) soil water content (SWC, θ) and (b) soil water pressure head (SWP) (absolute value in cm) during a day at six soil depths between observation (θ_{obs}, SWP_{obs}) and simulation (θ_{sim}, SWP_{sim}) by the Feddes–Jarvis (FJ) model, Feddes (F) model, Feddes model with parameters the same as the optimized parameters of the FJ model but with the critical water stress threshold $\omega_c = 1$ (F_{w1}), and Couvreur (C) model.

parameters, pressure heads in the Feddes stress function, and root-related parameters in the C model are illustrated in Fig. 5. Until early May, the actual RWU rate simulated by the models equaled the potential rate, gradually increasing from 0.05 to 0.2 cm d^{-1} (Fig. 5a). Then the potential RWU rate increased continuously in the period without sheltering (in the middle of May) and decreased in the middle of June. The actual RWU simulated by the FJ model with compensation was not able to meet the atmospheric demand from Week 12 (Fig. 5a), whereas without compensation the RWU was constrained 1 wk earlier. There was no water stress in the RWU simulated by the C model until Week 12. The delayed water stress in models with compensation is due to the fact that a local water limitation in soil implies a redistribution of water uptake but not necessarily a reduction of transpiration (as it would in the F and F_{w1} models). In the C model, any soil water potential variation with depth generates redistribution, as in a hydraulic network,

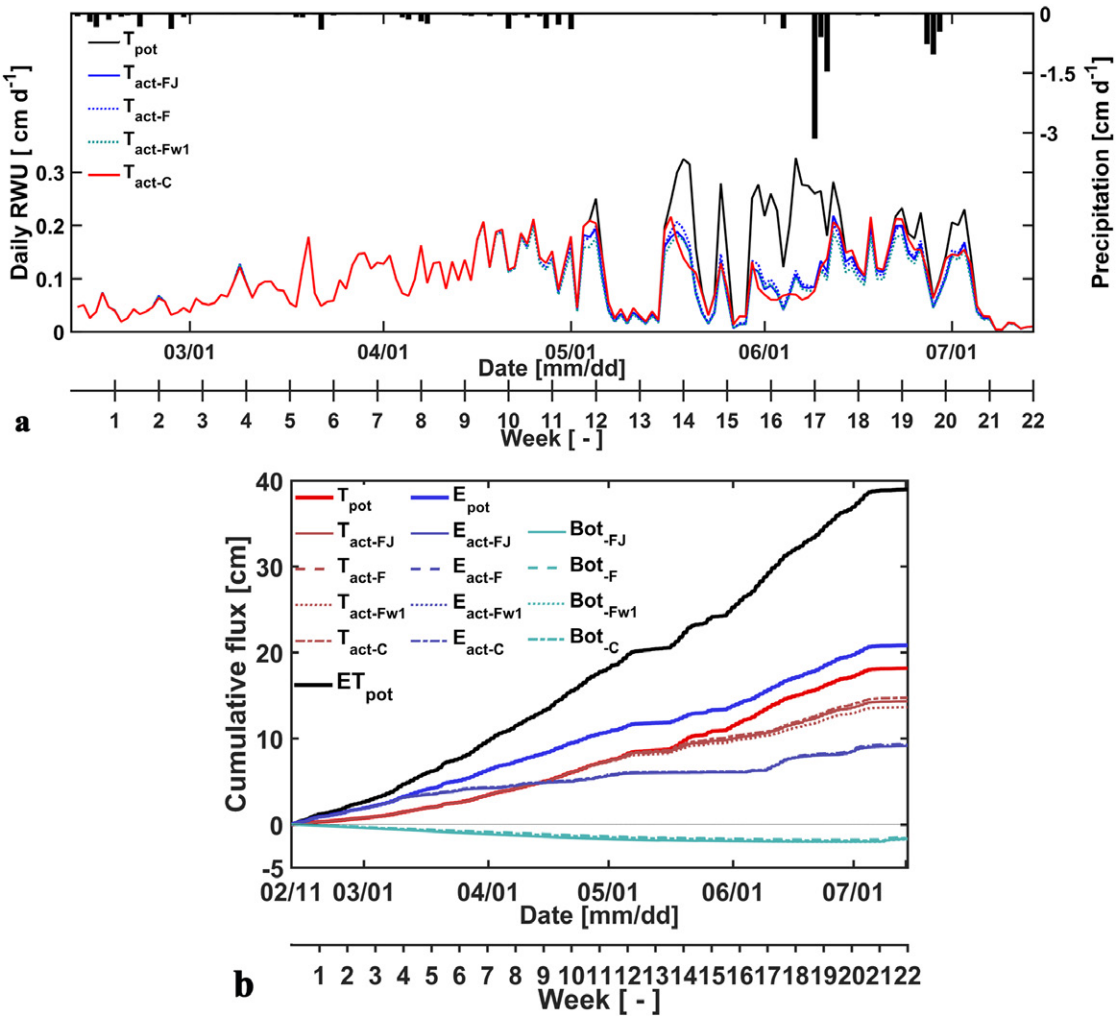

Fig. 5. (a) Comparisons between potential daily transpiration (T_{pot}) and root water uptake (RWU = actual transpiration, T_{act}) simulated by the Feddes–Jarvis (FJ) model, Feddes (F) model, Feddes model with parameters the same as the optimized parameters of the FJ model but with the critical water stress threshold $\omega_c = 1$ (F_{w1}), and Couvreur (C) model; and (b) comparison between cumulative potential evapotranspiration (ET_{pot}), T_{pot}, T_{act}, potential evaporation (E_{pot}), actual evaporation (E_{act}), and bottom flux (Bot) simulated by the FJ, F, F_{w1}, and C models during the whole period.

which tends to equilibrate the soil water potential and thus delays the occurrence of water stress more than in the FJ model. The estimated RWU by the FJ, F, and F_{w1} models followed the daily (or hourly, data not shown in the plots) variations of the T_{pot} during the water-stressed and unstressed periods, whereas for the C model, transpiration under water stress (e.g., from Weeks 14–18 in Fig. 5a) was higher before 12:00 PM as typically observed experimentally (Dodd et al., 2008). The cumulative actual RWU simulated by the FJ, F, and C models accounted for 78.84, 78.81 (75.08 for F_{w1}), and 81.11% of the cumulative potential water uptake, respectively, during the whole observation period (Fig. 5b). The estimated cumulative soil evaporation matched the cumulative potential soil evaporation until 9 March, when the falling-rate phase started. At the end of the observation, the cumulative evaporation simulated by the C model equaled that by the FJ model, but both were slightly (4 mm) lower than that simulated by the F model. The drainage simulated by the C model was slightly (2 mm) lower than that simulated by the F model from the middle of April to the middle of May, but there was no difference at the end of the simulation period. Water storage derived from SWC measurements and from simulations is shown in Fig. 6. The water storage derived from the observed SWC and simulations corresponded well except for a short time at the beginning, with 1.7 cm greater storage for the simulations. At the end of the optimization period, the simulated storage was 1 cm lower than that derived from the measurements. It should be noted that the observed storage was derived from interpolation of soil moisture measurements at six depths in the soil profile, which might be the reason for the deviations between the storage derived from simulations and measurements.

Overall, the measured and simulated data matched well for both models at the six soil depths. We did not observe systematic differences among the FJ, F, and C models. This can be seen in Supplemental Fig. S2, which shows the RMSE, ME, and *d* for the FJ, F, F_{w1}, and C models. The RMSE of SWC and SWP were no larger than 0.02 $cm^3\ cm^{-3}$ and 0.6 in pF [$\log_{10}(|h|\ cm)$] units,

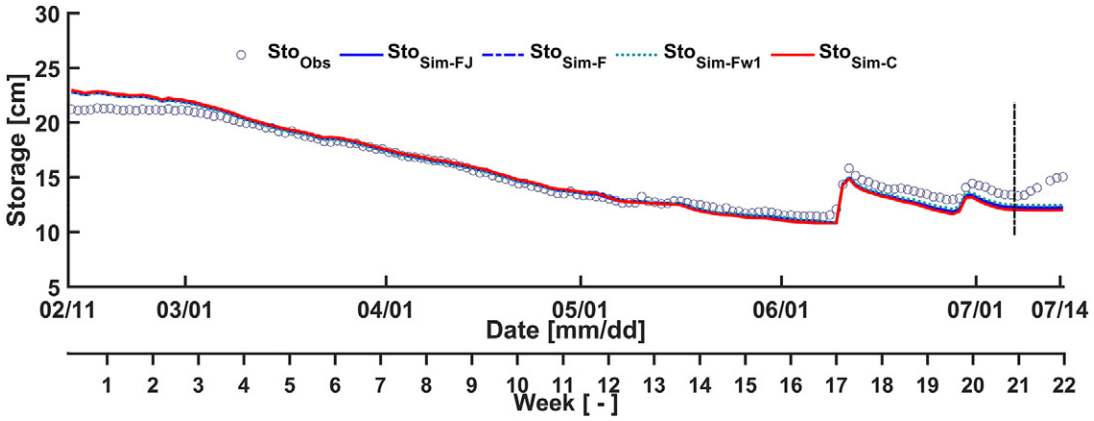

Fig. 6. Time evolution of the water storage (Sto) that was calculated from soil moisture measurements (Obs) and simulated (Sim) by the Feddes–Jarvis (FJ) model, Feddes (F) model, Feddes model with parameters the same as the optimized parameters of the FJ model but with the critical water stress threshold $\omega_c = 1$ (F_{w1}), and Couvreur (C) model.

respectively, indicating that the simulation errors were quite small. The distribution of ME showed that SWC at 20, 40, 60, and 120 cm was slightly ($\leq$0.02 cm^3 cm^{-3}) underestimated (SWP was overestimated by $\leq$0.4 pF units), and that the water storage was slenderly ($\leq$1 mm) overestimated. Also, the difference in water content (dSWC), water potential (dSWP), and water storage (dSto) were well predicted by all the models. The smaller coefficients of agreement, *d*, at greater depths are due to the small temporal changes at these depths.

Optimized Parameters of the Two Root Water Uptake Models

The optimized parameters of the FJ, F, and C models are listed in Table 3. The optimized soil hydraulic parameters that were obtained using the FJ model with compensation and using the C model were very similar but deviated from the soil parameters that were obtained when using the F model. The value of K_s was much smaller in the subsoil than in the topsoil. This may due to the high stone content with non-uniform size (Thoma et al., 2014) and the compaction of the soil during the construction of the plot (Cai et al., 2016). Novák et al. (2011) indicated that hydraulic conductivity decreased with increasing stone content but not to such a large extent. The parameter *l* was positive in the upper and negative in the lower soil layers. To some extent, negative *l* may be considered to be "unphysical" because it implies that tortuosity decreases when the soil dries out. Negative *l* was also obtained for other soils (e.g., Schaap and Leij, 2000; Yates et al., 1992), which shows that this parameter is rather a shape factor than a physically based parameter.

The obtained values of hCritA differed considerably among the different models but were considerably less negative than the commonly used values of −15,000 or −16,000 cm in RWU simulations. Pang et al. (2000) indicated that this value is soil texture related, being lower for fine materials and higher for coarse materials (around −5000 cm for sand or gravel). A sensitivity analysis showed that the simulation results were not affected when lower values of hCritA than the values in Table 3 were used.

The root uptake parameters h_{3l} and h_{3h} that were obtained using the FJ and F models were very similar and about 30% lower than the values suggested for wheat by Wesseling et al. (1991) (−500 and −900 cm). The critical water stress threshold ω_c in the FJ model was 0.8, which is consistent with the speculation of Šimůnek and Hopmans (2009) that ω_c is relatively high for cultural plants compared with natural plants because the cultural plants have limited ability to compensate stress. For the C model, the optimized K_{rs_ini} is about a factor of 4 larger than K_{comp_ini} (Fig. 7), which is also indicative of a relatively small RWU compensation. Both K_{rs} and K_{comp} increased by a factor of 6.3 (which is the ratio of

Table 3. Optimized soil hydraulic parameters, including saturated hydraulic conductivity ($K_{s1,2}$) and empirical coefficient ($l_{1,2}$) in the top- and subsoil, minimum pressure head at the soil surface (hCritA), pressure heads at high (h_{3h}) and low (h_{3l}) transpiration rates, and the critical water stress threshold ω_c and initial root system (K_{rs_ini}) or compensatory (K_{comp_ini}) root water uptake conductance in the Feddes (F), Feddes–Jarvis (FJ), and Couvreur (C) models.

Model	K_{s1}	l_1	K_{s2}	l_2	hCritA	h_{3l}	h_{3h}	ω_c	K_{rs_ini}	K_{comp_ini}
	cm h^{-1}		cm h^{-1}		cm				h^{-1}	
FJ	3.417	1.470	0.026	−2.797	−7434	−1172	−648	0.8	–	–
F	2.529	1.084	0.015	−3.274	−5633	−1194	−685	1 (fixed)	–	–
C	3.853	1.472	0.021	−2.892	−9120	–	–	–	3.792×10^{-7}	1.125×10^{-7}

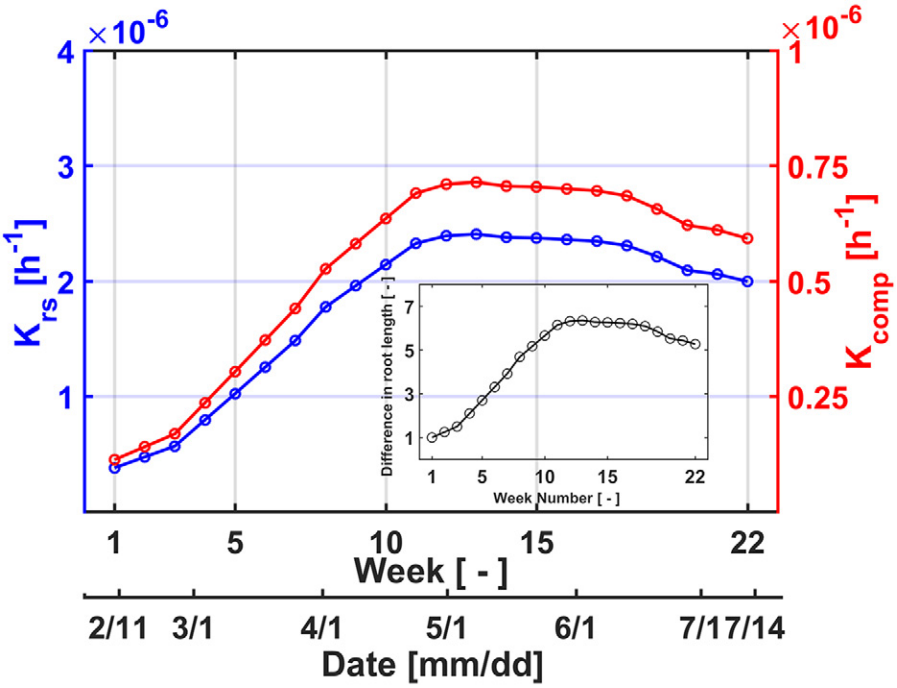

Fig. 7. Estimated equivalent conductance of the root system (K_{rs}) and compensatory root water uptake conductance of the roots (K_{comp}) during 22 wk. The inset shows the relative difference in root length between the first week and the following weeks.

maximum to initial root length) during the growth period, at the end of which the values decreased slightly due to root senescence.

To evaluate the uniqueness of the parameters found by the GA optimization and whether the GA algorithm found the global optimum, selected response surfaces are shown in Fig. 8. Considering the soil hydraulic parameters, the response surfaces showed clear minima, indicating that the parameters were identifiable (Fig. 8a–8c). Also, the parameters of the C model were identifiable (Fig. 8d–8f). However, for the parameters h_{3h} and h_{3l} of the F and FJ models (Fig. 8g–8h), the response surface did not show a distinct minimum, while a minimum could be observed for ω_c (Fig. 8i) in the response surface.

The root system hydraulic conductance, K_{rs}, can also be measured directly in the laboratory or in field experiments by a high-pressure flow meter (Judd et al., 2016; Tyree et al., 1995) or a pressure chamber (Miyamoto et al., 2001). However, these measurements were restricted to extracted root systems and, for crops, the measurements were mostly performed on young roots of seedlings. The values obtained from those studies could therefore not be compared with the inversely estimated values in this study due to different root development. Alternatively, K_{rs} and K_{comp} can be calculated directly from the root architecture and the hydraulic properties of root segments. Couvreur et al. (2014) calculated K_{rs} and K_{comp} of winter wheat by virtually reconstructing its hydraulic architecture using literature data. The architecture was generated with the model Root Typ (Pagès et al., 2004), accounting for plant-specific root traits and reproducing RLD profiles observed in early spring. Radial and axial conductivities changing with root segment age were also accounted for. The conductance values derived from these calculations represent the conductance of a single plant, whereas K_{rs} used in the one-dimensional model represents the conductance of the root systems per unit area of the upper soil surface. To match the units, K_{rs} obtained from calculations was divided by the root length of the virtual plant and K_{rs} obtained from inverse modeling was divided by the total root length under a horizontal unit surface area, which corresponds to the depth integral of the RLD (Fig. 9a). Therefore, observations of root numbers or root lengths in the rhizotubes had to be transformed to RLDs.

We considered two approaches that make different assumptions about the distribution of roots in the soil around rhizotubes (Fig. 9b). The first one uses the root length that is observed in the images and an empirical soil thickness of 2 mm. This approach assumes that the volume of the rhizotube has no impact on the RLD that is observed in a small soil volume at the lateral sides of the rhizotubes. The second option uses the root counts from the images. It assumes that all roots that impact on the walls of the rhizotube grow along the rhizotube surface and are detected at the lateral sides. When it is further assumed that roots would grow nearly vertically in the absence of the rhizotube, the projected root length equals the number of intercepted roots times the diameter of the rhizotube. Considering a planting density of 310 plants m^{-2}, the calculated total root length per plant in Week 8 when roots were first observed at 80 cm was 47.20 and 5.77 m from observed lengths and observed impacts, respectively. This range represents an uncertainty range of the actual root length of a plant that is estimated from rhizotube images. This range could be narrowed when using a calibration of the rhizotube observations against direct observations of RLD. With the root architecture model, a root length of 43.56 m per plant and a rooting depth of 95 cm was obtained (data were from Couvreur et al., 2014). The K_{rs} derived from the architecture model was 0.0152 $cm^2\ d^{-1}$ (data from Couvreur et al., 2014) for a single plant, and K_{rs} obtained in this study was $1.8 \times 10^{-6}\ h^{-1}$ in Week 8. Consequently, the root hydraulic conductance per unit root length was 1.23×10^{-8} and 1.01×10^{-7} cm h^{-1} for Week 8 and 1.48×10^{-7} cm h^{-1} for the root architecture model.

When comparing the root conductance values obtained from inverse modeling and the root architecture model, it must be considered that the root architecture model was not calibrated

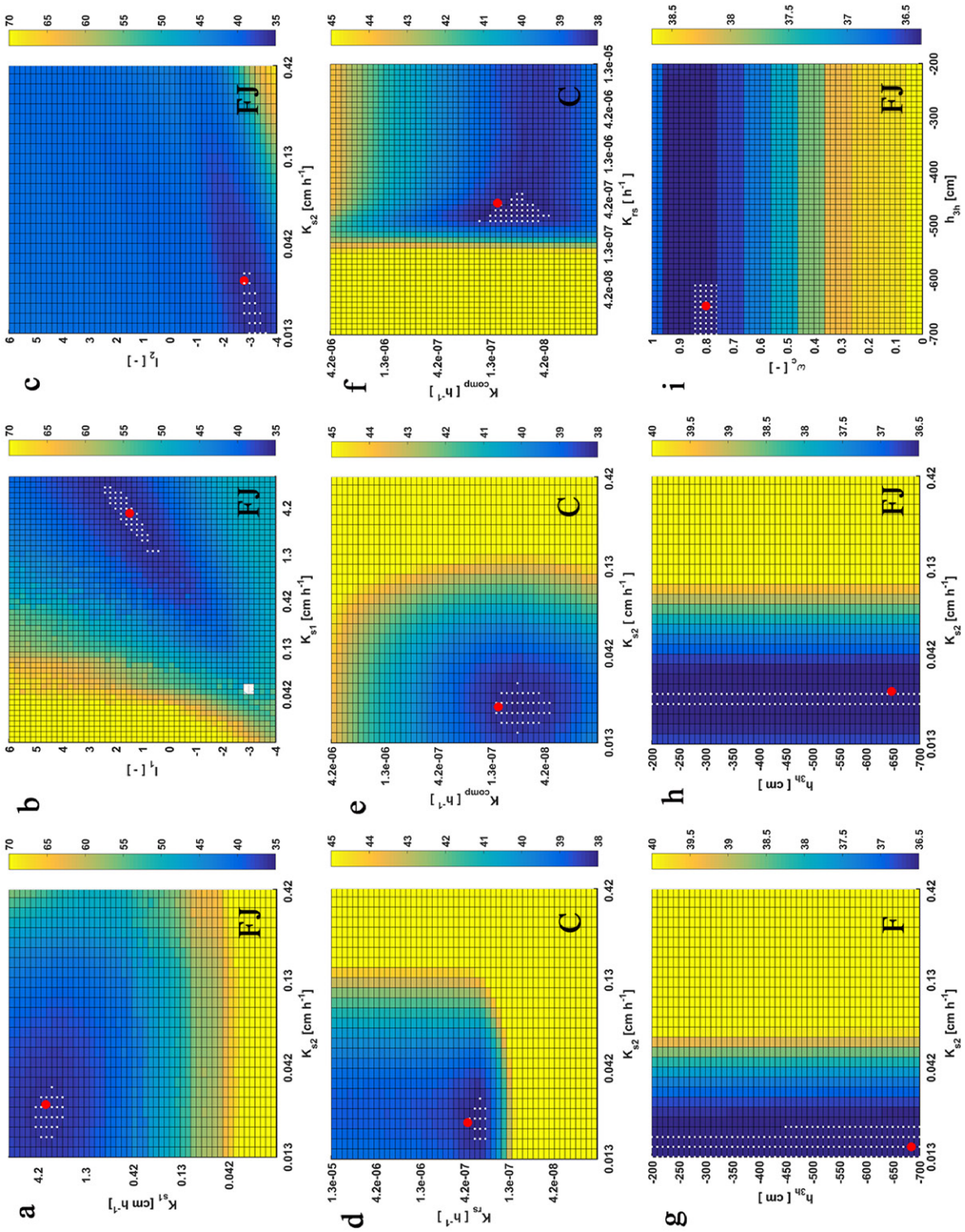

Fig. 8. Using the Feddes–Jarvis (FJ) model, Feddes (F) model with parameters the same as the optimized parameters of the FJ model but with the critical water stress threshold $\omega_c = 1$ (F_{w1}), and Couvreur (C) model, response surfaces for (a) K_{s2} vs. K_{s1}, (b) K_{s1} vs. l_1, (c) K_{s2} vs. l_2, (d) K_{s2} vs. K_{rs}, (e) K_{s2} vs. K_{comp}, (f) K_{rs} vs. K_{comp}, (g) K_{s2} vs. h_{3h}, (h) K_{s2} vs. h_{3h}, and (i) h_{3h} vs. ω_c parameter planes, where K_s is saturated conductivity; l is an empirical model parameter; subscripts 1 and 2 denote the top- and subsoil, respectively; K_{rs} is equivalent conductance of the root system; K_{comp} is compensatory root water uptake conductance; h_{3h} is water potential at high transpiration; and ω_c is a root adaptability factor. The color bar indicates the range of the objective function, the white dot is the area within a 0.5% range of the objective function minimum, and the red dot is the optimum value obtained from inverse modeling.

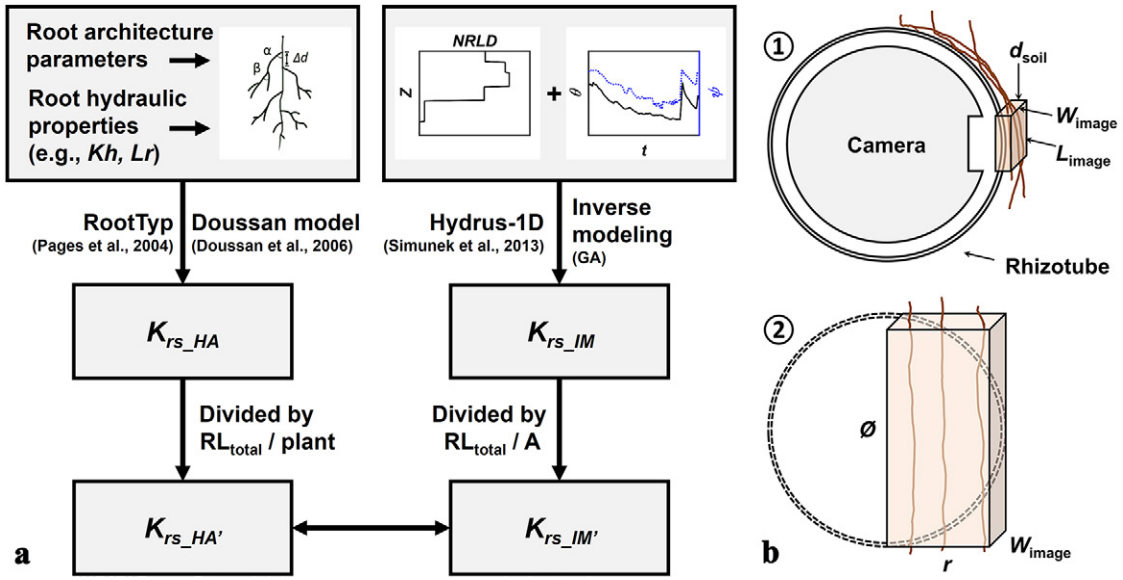

Fig. 9. (a) Deriving root hydraulic conductance from the architecture model and the inverse modeling, and (b) options for calculating root length density from the rhizotube: (1) uses the root length that is observed in the images and an empirical soil thickness of 2 mm and (2) uses the root counts from the images; Kh and Lr are root axial conductance ($cm^3\ d^{-1}$) and radial conductivity (d^{-1}), NRLD is normalized root length density, K_{rs_HA} and K_{rs_IM} are root hydraulic conductance derived from the architecture model ($cm^2\ d^{-1}$) and inverse modeling (h^{-1}), RL_{total} is root length of a single plant (cm), A is the horizontal soil area per plant (cm^2), d is the observed soil thickness (cm), W and L are width and length of the effectively observed volume (cm), and ∅ and r are diameter and radius of the rhizotube (cm).

for this specific soil with a high stone content and for the water stress conditions in the experiments but used root-related parameters from the literature. Furthermore, there is uncertainty about the translation of the inverted root conductance values to a root conductance per unit root length that is related to the interpretation of the rhizotube measurements. As a consequence, the fact that the order of magnitude of the derived parameters corresponds indicates that the inversely estimated root conductance values are consistent with properties of the root system that can be measured directly.

Different from what was obtained in the numerical modeling, K_{comp} was much lower than K_{rs} in this study. The smaller K_{comp} limited compensatory RWU, although it remained quite significant as shown by the changing shape of the RWU profile (discussed below). The value of K_{comp} could be equal to K_{rs} if axial resistance is much lower than radial resistance; however, the difference between the two parameters becomes larger when the root axial conductance decreases (Couvreur et al., 2012). Roots may lose contact with the soil when the soil dries out, which will lead to a lower redistribution to drier soil layers (Carminati et al., 2009), which also accounts for the lower K_{comp}. Besides, we assumed that the uptake is proportional to the RLD. However, the radial conductance of root segments decreases when they grow older. Therefore, the sink term and compensatory uptake may be smaller in regions where the roots are, on average, older. Given the complexity of realistic root hydraulic properties, these two parameters should best be considered as two independent variables for other crop species in future investigations to grant an extra degree of freedom to the model, especially when the root axial conductance is relatively low (Couvreur et al., 2012).

Effect of Soil Hydraulic Parameters

For a saturated conductivity in the lower soil layer of 0.02 cm h^{-1}, which was close to the optimized K_{s2} of the C model, the F_{w1} model predicted about 7% less uptake than the C model and 5% less than the FJ model (Fig. 10). These results demonstrate the effect of considering RWU compensation on the cumulative RWU in this study. The obtained K_{s2} in the subsoil was very low, but, for all models, the simulated uptake increased with increasing K_{s2}. These results indicate that the amount of water retained in the soil profile was sufficiently large to satisfy the potential uptake but the uptake in this soil was limited by the soil hydraulic conductivity that prevented water redistribution in the soil profile. The root system could compensate only partly for this limited redistribution.

Root Water Uptake Profiles Simulated by the Different Models

Similar soil moisture distributions and cumulative uptake were estimated by the FJ model (also F_{w1}) and the C models. We investigated whether simulated RWU distributions differed among the different models. Figure 11 shows the RWU distributions simulated by the FJ, F_{w1}, and C models and the root distributions along the soil profile during a 24-h period in Weeks 11 (no water stress in the C model but stress started in the F model), 15 (in the stress period), and 18 (a day before water stress ended and after a rainfall event). The spatiotemporal variations of RWU that were simulated

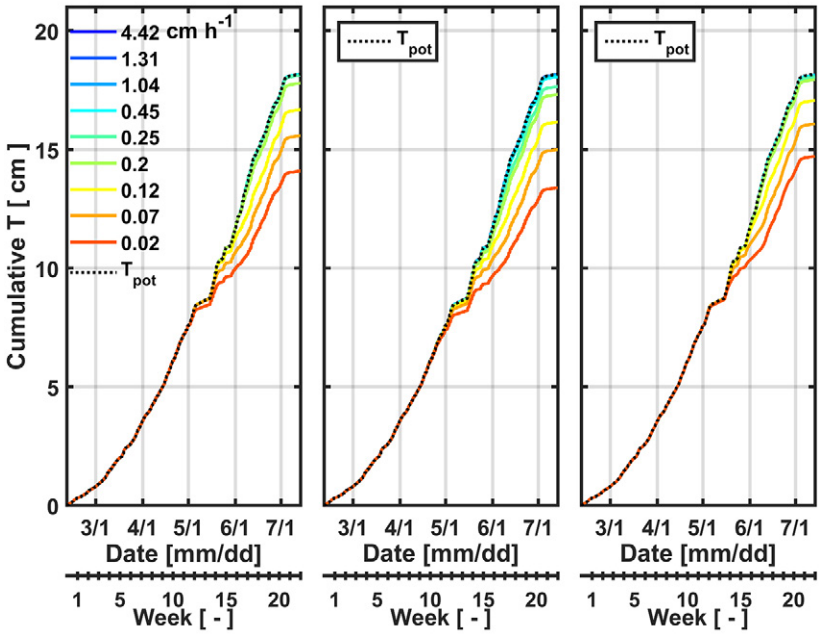

Fig. 10. The cumulative root water uptake (RWU = T) simulated by the Feddes–Jarvis (FJ) model (critical water stress threshold ω_c = 0.8, left), Feddes model with parameters the same as the optimized parameters of the FJ model except ω_c = 1 (middle), and Couvreur model (right) with different saturated hydraulic conductivity K_s values in the subsoil; also shown is potential transpiration (T_{pot}).

by the FJ, F_{w1}, and C models along the soil profile were similar in Week 11. The water uptake profile simulated by the models followed the spatial root distribution: when there was no water stress, RWU was higher in the soil layers where NRLD was higher, as observed by Adiku et al. (2000) and de Willigen et al. (2012). The water uptake simulated by the FJ and F_{w1} models stopped at night; however, for the C model, soil water was taken from the 40- to 70-cm depth and released from 10 to 40 cm between 10:00 PM and 5:00 AM. In the C model, compensation is considered to be the internal adjustment of water uptake and happens even when there is no water stress but with nonuniform distribution of water potentials within the root zone (Couvreur et al., 2012; Javaux et al., 2013).

Water depletion and a reduction in water uptake occurred first in the layers from 15- to 50-cm depth. It should be noted that also in the layer from 50- to 70-cm depth the uptake rate was high before the onset of stress (or at the early stage of water stress, e.g., Week 12). However, this layer could be replenished by water from deeper soil layers, as is also evidenced by the greater uptake at the bottom of this layer during Week 15. After the irrigation and rainfall events during Week 18, the water uptake rate increased again and became equal to the potential uptake rate in the upper soil layer from the 0- to 40-cm depth, whereas uptake was still reduced at 40 to 70 cm. The dry conditions in the deeper soil layers prevented the crop transpiration from returning to the potential transpiration rate immediately after irrigation and precipitation (see also Fig. 5a).

Comparing the simulated RWU by the FJ and F_{w1} models when RWU from the layer at roughly the 15- to 50-cm depth was reduced, RWU compensation in the FJ model resulted in a higher RWU from the deeper soil layers but also from the soil layer between 0 and 15 cm. Despite these differences, the RWU profiles simulated by the FJ and F_{w1} models were very similar and differed considerably from the uptake profiles simulated by the C model (Fig. 11). The FJ and F_{w1} models did not simulate RWU at night, whereas in the C model, uptake from wetter regions in the root zone continued at night and the absorbed water was released again in drier soil layers. This process is called *hydraulic lift* when water is released in shallow layers (Caldwell et al., 1998; Neumann and Cardon, 2012; Richards and Caldwell, 1987). Interestingly, the C model also simulated absorption from shallower layers after a rainfall event and a release in deeper, drier layers (Week 18). Such an inverse hydraulic redistribution has also been reported in both woody and grass plant root systems (Bleby et al., 2010; Leffler et al., 2005). The redistribution of water through the root system at night also had an impact on the simulated RWU profiles during the day. Water that was released in dry soil layers during the night was taken up during the next day so that the water uptake during the day was more equally distributed throughout the root profile than in the FJ and F_{w1} models.

To evaluate the effects of the difference in diurnal dynamics of RWU that is simulated by the different models, simulated transpiration rates and soil water contents during Week 15 are shown in Fig. 12. The C model simulated smaller peak RWU rates but larger RWU rates, which equaled the potential ones, during the morning and evening than the FJ and F_{w1} models. The C model simulated the largest water release at night at 40 cm; the release and subsequent uptake of water (7.7×10^{-5} h^{-1} at 10:00 PM in Fig. 11) was quite small and the corresponding variation in SWC was 0.002 cm^3 cm^{-3}, which was too small to be detected by the soil moisture sensors (Fig. 12b). This small variation in SWC due to the water redistribution by roots to the dry soil has also been indicated by other researchers. Zegada-Lizarazu and Iijima (2004) investigated 16 food crops using deuterium labeling, and the results showed that for a wheat crop, the deuterium concentration (delta notation) was increased by 0.003% during the night in the topsoil (up to 25 cm) through hydraulic lift. Shen et al. (2011) indicated that SWC increased 0.01 to 0.02 cm^3 cm^{-3} in the dry and upper soil (up to 15 cm) at night during the blooming stage of winter wheat through hydraulic lift. Guderle and Hildebrandt (2015) simulated an increase in SWC around 0.003 cm^3 cm^{-3} using an exponential root growth model and synthetic data. The changes in SWC and SWP during the compensatory process were too small to be detected using soil moisture sensors. However, water isotope

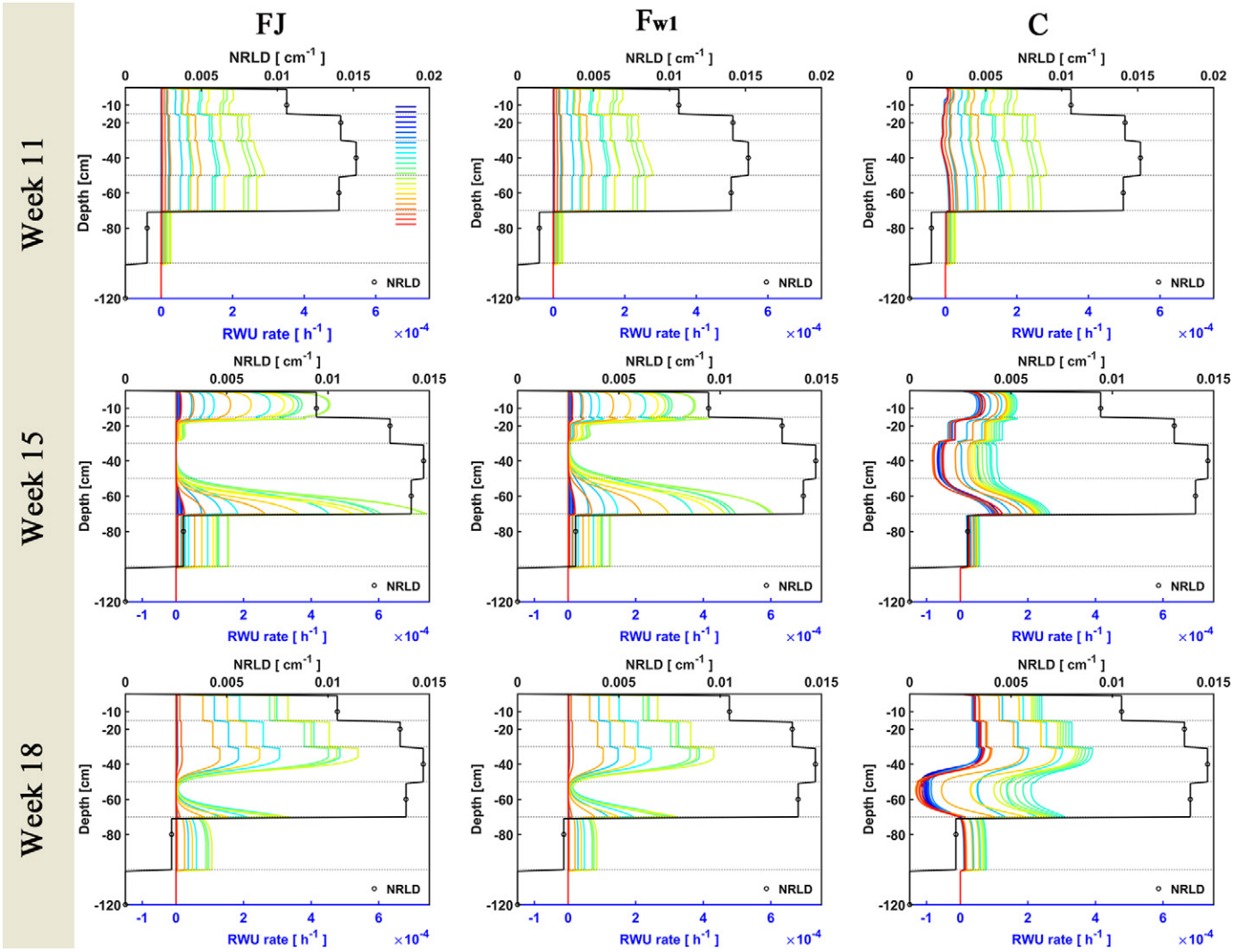

Fig. 11. Normalized root length density (NRLD, black lines) and root water uptake (RWU) rate (colored lines) simulated by the Feddes–Jarvis (FJ) model, Feddes (F) model, Feddes model with parameters the same as the optimized parameters of the FJ model but with the critical water stress threshold $\omega_c = 1$ (F_{w1}), and Couvreur (C) model in 24 h of Week 11, 15, and 18 along the soil profile. The corresponding dates are 22 Apr., 20 May, and 13 June 2014. The legend for the 24 h is represented by the color from blue (1 h) to red (24 h).

tracing techniques could be applied to determine the magnitude of hydraulic lift and RWU compensation and deliver relevant information to parameterize RWU models (Rothfuss and Javaux, 2016). This information could be supplemented by information about the diurnal transpiration dynamics obtained from sap flow measurements (Langensiepen et al., 2014).

Relation between Root Water Uptake and Soil Water Pressure Head

Figure 13 shows how the simulated ratio of actual to potential transpiration (Fig. 13a) and the actual transpiration during stress periods (Fig. 13b) are related to the effective soil water potential in the root zone, h_{Te}, for the different models. Only actual transpiration rates at 12:00 PM are shown. These functions represent root-system- or plant-scale stress functions that relate the total RWU to an effective water potential in the root zone, h_{Te}. Because the potential transpiration rates at 12:00 PM were mostly >0.02 cm h^{-1} (Fig. 2), the h_3 parameter for the Feddes reduction function α_F was mostly equal to h_{3h}. This explains why, for the FJ model, all points in the T_{act}/T_{pot} vs. h_{Te} plot fall nearly on a line. For the F and F_{w1} models without RWU compensation, the line is equal to the α_F function for the high transpiration rate. However, RWU compensation shifts the line toward more negative h_{Te} values, demonstrating that compensation leads a lower reduction in actual transpiration for a given h_{Te} and to a more negative h_{Te} when stress onset occurs than the threshold h_3 in the α_F function (which was −648 cm for the FJ model, see Table 3). This demonstrates that when root water compensation occurs, the local stress function α_F cannot be derived from a plant-scale stress function that could be derived directly from measuring plant transpiration and pressure heads in the root zone. In the C model, during water limitation, the relation between T_{act}/T_{pot} and h_{Te} is linear but with a slope that is proportional to K_{rs}/T_{pot} (see Eq. [13]), which explains the scatter in Fig. 13a (in which red lines correspond to different T_{pot}

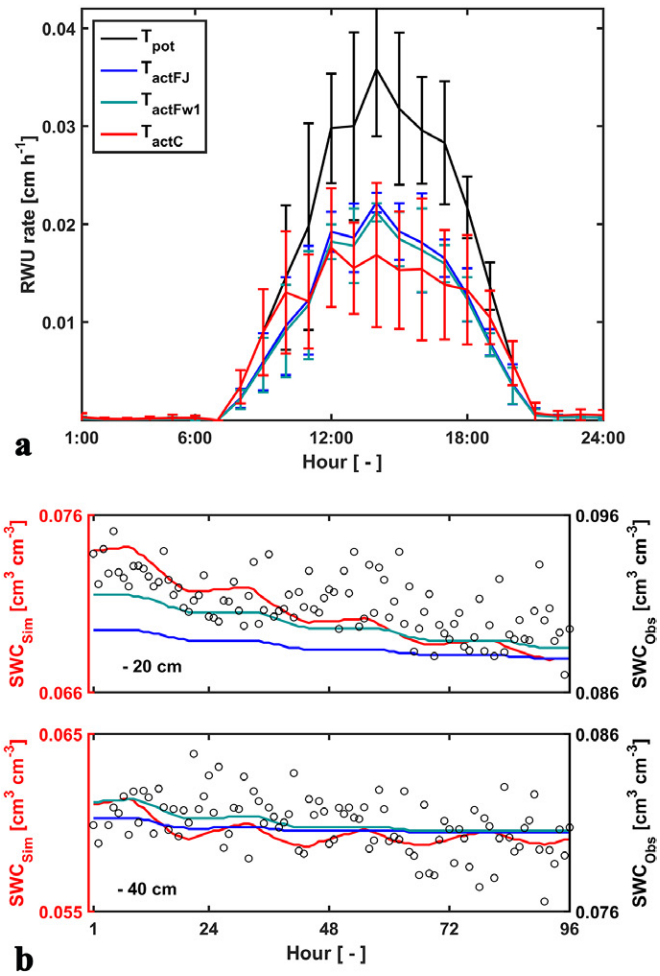

Fig. 12. (a) Variations of potential transpiration (T_{pot}) and diurnal averaged root water uptake (RWU = T_{act}) simulated by the Feddes–Jarvis (FJ) model, Feddes model with parameters the same as the optimized parameters of the FJ model but with the critical water stress threshold ω_c = 1 (F_{w1}), and Couvreur (C) model, and (b) observed hourly soil water content (SWC) vs. SWC simulated by the FJ, Fw1, and C models at the 20- and 40-cm depths from 17 May to 20 May 2014 (Week 15).

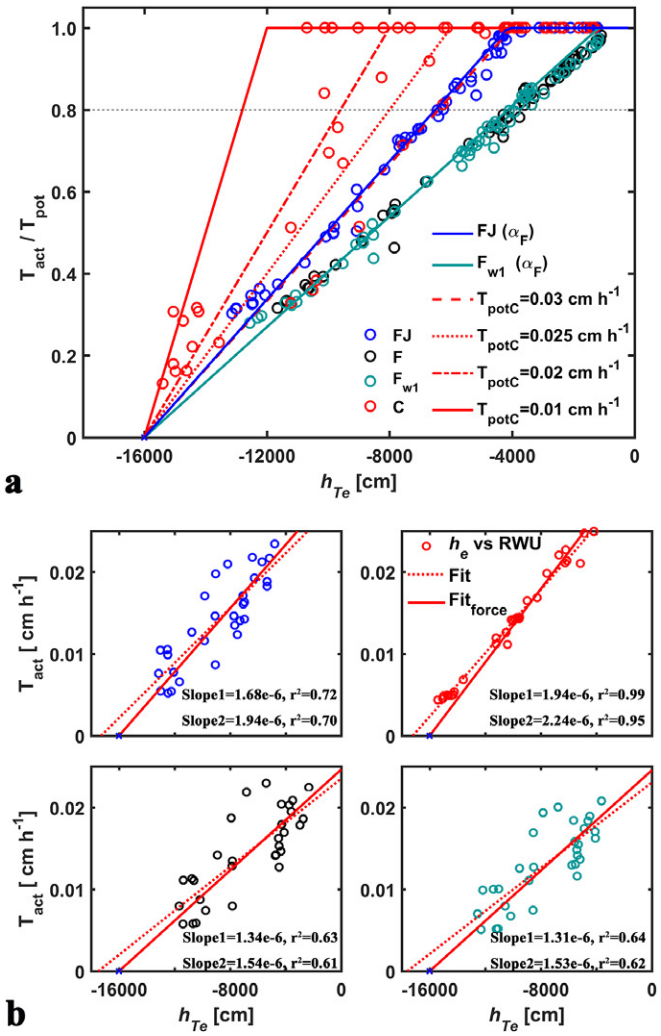

Fig. 13. (a) The relation between effective soil hydraulic head (h_{Te}) and relative root water uptake (RWU = actual transpiration T_{act}/potential transpiration T_{pot}) that was simulated by the Feddes–Jarvis (FJ) model, Feddes (F) model, Feddes model with parameters the same as the optimized parameters of the FJ model but with the critical water stress threshold ω_c = 1 (F_{w1}), and Couvreur (C) model (circles), calculated by the Feddes stress function (α_F) using the optimized water potential at high (h_{3h}) and low (h_{3l}) transpiration, and calculated by the C model using the mean root system conductance K_{rs} (Weeks 11–21) and different T_{pot} values; and (b) the relation between the effective soil hydraulic head h_{Te} and T_{act} simulated by the FJ, F, F_{w1}, and C models during water-stress periods for h_{Te} selected at 12:00 PM (data in the sheltered periods not included). Slope 1 (dashed line) and slope 2 (solid line) denote the slopes of the fitted curve and the fitted curve with forcing through the point (−16000, 0), respectively.

values). It is interesting to note that for T_{pot} = 0.03 cm h^{-1} and K_{rs} = 2.5 × 10^{-6} h^{-1}, which are representative for the maximum T_{pot} and the root system conductance during the considered period, respectively, the relation between T_{act}/T_{pot} and h_{Te} predicted by the C model is similar to the one obtained for the FJ model (Fig. 13a). This suggests that proxies of the C model parameters may be inferred from the FJ model parameter libraries (Couvreur et al., 2014a). When T_{act} during stress periods is plotted vs. h_{Te}, a linear relation is obtained for the C model (Fig. 13b). For the FJ and F models, the points are scattered. In the Feddes models (FJ and F), the relation between T_{act}/T_{pot} and h_{Te} can be made a function of T_{pot} by making h_3 a function of T_{pot}. However, the maximum value of T_{pot} for which h_3 varied (0.02 cm h^{-1}) was smaller than the T_{pot} values at 12:00 PM that were considered so that there was, in fact, no dependence on T_{pot} in the relation between T_{act}/T_{pot} and h_{Te} shown in Fig. 13a. This led to the scatter in the relation between T_{act} and h_{Te} for the Feddes models (FJ and F) in Fig. 13b. However, for the FJ model, the points scattered around the relation that was obtained for the C model so that both models simulated, on average, the same relation between T_{act} and h_{Te}.

Summary and Conclusions

This study compared the soil moisture prediction and the performance of RWU with different compensation by the coupled FJ, F,

and C RWU models in the HYDRUS-1D framework with in situ observations from a minirhizotron facility. Soil hydraulic parameters and RWU parameters of the three models could be estimated using observations of soil water content, potential, and root distribution. The three models could describe the observations equally well. The same soil hydraulic properties were obtained for the two models that considered RWU compensation. The F model without considering compensation could describe the observation data, but slightly different soil parameters were obtained. If the same soil hydraulic parameters were used in the FJ model as in the models that considered RWU compensation, less RWU was simulated by the F_{w1} model. However, RWU compensation increased the total water uptake only to a small extent and was not able to avoid water stress. A sensitivity analysis demonstrated that the amount of water in the soil profile would be sufficient to avoid water stress but the hydraulic conductivity of the soil profile limited the redistribution of water in the root zone that would be necessary to avoid water stress.

The obtained RWU parameters were consistent with data reported in the literature. Response surfaces of the objective function showed that the root-related parameters of the C model could be identified using inverse modeling. Furthermore, these parameters were consistent with simulations using root architecture models and the hydraulic parameters of roots. However, for the F and FJ models, the RWU parameters that define the onset of water stress as a function of the soil water pressure, h_{3l} and h_{3h}, could not be uniquely identified.

The obtained root parameters were indicative of limited RWU compensation. The C and FJ models simulated similar (C was 2.8% more) total RWU; however, they predict different diurnal dynamics of local RWU. The C model predicted water exudation at night in dry soil layers (hydraulic lift or hydraulic redistribution). The exuded water was taken up during the next day so that the net water uptake from the dry layers was zero and equal to the uptake predicted by the FJ model. The amount of water that was released at night was, however, too small to be detected by soil moisture sensors. Although there is evidence from isotope trace studies that this process is taking place, it remains questionable whether this process is relevant for RWU for longer periods.

Although the RWU compensation functions of the FJ and C models arise from different approaches and the nature of their parameters differs, they predicted similar plant- or root-system-scale stress functions, which opens possibilities of parameter transfer between the two models. The root-system-scale stress functions deviate due to RWU compensation from the local stress functions that are used in the FJ model. The close agreement in root-system-scale stress functions between the FJ and C models was due to the more or less constant root system conductance during the period when the stress occurred. The C model links the stress function to the root system conductance, which in turn depends on the development of the root system. As a consequence, this model will predict different root-system-scale stress functions at different stages during the growing season and will also predict different stress functions for plants growing in different soils in which the root system development is different. Similarly, Vandoorne et al. (2012) indicated that the parameters h_{3l} and h_{3h}, which are assumed to remain constant during the growing season (Feddes et al., 1978) in the Feddes stress function, were "not unique for a given plant" and differed between different periods in the growing season of chicory (*Cichorium intybus* L.). This implies that the stress function parameters in the FJ model should be a function of the crop development stage and root system status. As a consequence, these parameters should be adapted depending on the development of the root system. However, a function that links the stress parameters to root system parameters is lacking.

Acknowledgments

This study was financially supported by SFB/TR 32 (Transregional Collaborative Research Centre 32, funded by the Deutsche Forschungsgemeinschaft [DFG]). The rhizotron facility is part of the TERENO network of terrestrial observatories. We are grateful to Hubert Hüging and Matthias Langensiepen for taking care of the crops, fertilizers, and herbicides. We thank Jirka Šimůnek for providing the new version of HYDRUS-1D and the project TERENO for providing the meteorological data. During the preparation of this manuscript, V. Couvreur was supported by the Belgian American Educational Foundation (BAEF) as a UCLouvain Fellow, by Wallonie-Bruxelles International (WBI) with a WBI.WORLD excellence grant, and by the Fonds Spéciaux de Recherche (FSR) of the Université catholique de Louvain. We sincerely thank the reviewers for constructive criticisms and valuable comments, which were of great help in revising the manuscript.

Supplemental Material

The supplemental material online includes a comparison of the difference in SWC and the difference in SWP between observations and simulations and a statistical analysis of the simulated results at six soil depths using all four models.

References

Adiku, S.G.K., C.W. Rose, R.D. Braddock, and H. Ozier-Lafontaine. 2000. On the simulation of root water extraction: Examination of a minimum energy hypothesis. Soil Sci. 165:226–236. doi:10.1097/00010694-200003000-00005

Albasha, R., J.-C. Mailhol, and B. Cheviron. 2015. Compensatory uptake functions in empirical macroscopic root water uptake models–Experimental and numerical analysis. Agric. Water Manage. 155:22–39. doi:10.1016/j.agwat.2015.03.010

Allen, R.G., L.S. Pereira, D. Raes, and M. Smith. 1998. Crop evapotranspiration: Guidelines for computing crop water requirements. Irrig. Drain. Pap. 56. FAO, Rome.

Asseng, S., J. Ritchie, A. Smucker, and M. Robertson. 1998. Root growth and water uptake during water deficit and recovering in wheat. Plant Soil 201:265–273. doi:10.1023/A:1004317523264

Baram, S., V. Couvreur, T. Harter, M. Read, P.H. Brown, M. Kandelous, et al. 2016. Estimating nitrate leaching to groundwater from orchards: Comparing crop nitrogen excess, deep vadose zone data-driven estimates, and HYDRUS modeling. Vadose Zone J. 15(11). doi:10.2136/vzj2016.07.0061

Bleby, T.M., A.J. Mcelrone, and R.B. Jackson. 2010. Water uptake and hydraulic redistribution across large woody root systems to 20 m depth. Plant Cell Environ. 33:2132–2148. doi:10.1111/j.1365-3040.2010.02212.x

Borg, H., and D. Grimes. 1986. Depth development of roots with time: An empirical description. Trans. ASAE 29:194–197. doi:10.13031/2013.30125

Cai, G., J. Vanderborght, A. Klotzsche, J. van der Kruk, J. Neumann, N. Hermes, and H. Vereecken. 2016. Construction of minirhizotron facilities for investigating root zone processes. Vadose Zone J. 15(9). doi:10.2136/vzj2016.05.0043

Caldwell, M.M., T.E. Dawson, and J.H. Richards. 1998. Hydraulic lift: Consequences of water efflux from the roots of plants. Oecologia 113:151–161. doi:10.1007/s004420050363

Carminati, A., D. Vetterlein, U. Weller, H.-J. Vogel, and S.E. Oswald. 2009. When roots lose contact. Vadose Zone J. 8:805–809. doi:10.2136/vzj2008.0147

Carsel, R.F., and R.S. Parrish. 1988. Developing joint probability distributions of soil water retention characteristics. Water Resour. Res. 24:755–769. doi:10.1029/WR024i005p00755

Couvreur, V., J. Vanderborght, L. Beff, and M. Javaux. 2014. Horizontal soil water potential heterogeneity: Simplifying approaches for crop water dynamics models. Hydrol. Earth Syst. Sci. 18:1723–1743. doi:10.5194/hess-18-1723-2014

Couvreur, V., J. Vanderborght, X. Draye, and M. Javaux. 2014a. Dynamic aspects of soil water availability for isohydric plants: Focus on root hydraulic resistances. Water Resour. Res. 50:8891–8906. doi:10.1002/2014WR015608

Couvreur, V., J. Vanderborght, and M. Javaux. 2012. A simple three-dimensional macroscopic root water uptake model based on the hydraulic architecture approach. Hydrol. Earth Syst. Sci. 16:2957–2971. doi:10.5194/hess-16-2957-2012

Deb, S.K., M.K. Shukla, and J.G. Mexal. 2011. Numerical modeling of water fluxes in the root zone of a mature pecan orchard. Soil Sci. Soc. Am. J. 75:1667–1680. doi:10.2136/sssaj2011.0086

De Faria, R., C. Madramootoo, J. Boisvert, and S. Prasher. 1994. Comparison of the versatile soil moisture budget and SWACROP models for a wheat crop in Brazil. Can. Agric. Eng. 36:57–68.

de Jong van Lier, Q., J.C. van Dam, A. Durigon, M.A. dos Santos, and K. Metselaar. 2013. Modeling water potentials and flows in the soil–plant system comparing hydraulic resistances and transpiration reduction functions. Vadose Zone J. 12(3). doi:10.2136/vzj2013.02.0039

de Jong van Lier, Q., J.C. van Dam, K. Metselaar, R. de Jong, and W.H.M. Duijnisveld. 2008. Macroscopic root water uptake distribution using a matric flux potential approach. Vadose Zone J. 7:1065–1078. doi:10.2136/vzj2007.0083

de Willigen, P., J.C. van Dam, M. Javaux, and M. Heinen. 2012. Root water uptake as simulated by three soil water flow models. Vadose Zone J. 11(3). doi:10.2136/vzj2012.0018

Dodd, I.C., G. Egea, and W.J. Davies. 2008. Abscisic acid signalling when soil moisture is heterogeneous: Decreased photoperiod sap flow from drying roots limits abscisic acid export to the shoots. Plant Cell Environ. 31:1263–1274. doi:10.1111/j.1365-3040.2008.01831.x

Dong, X., B.D. Patton, A.C. Nyren, P.E. Nyren, and L.D. Prunty. 2010. Quantifying root water extraction by rangeland plants through soil water modeling. Plant Soil 335:181–198. doi:10.1007/s11104-010-0401-7

Doussan, C., L. Pagès, and G. Vercambre. 1998. Modelling of the hydraulic architecture of root systems: An integrated approach to water absorption—Model description. Ann. Bot. 81:213–223. doi:10.1006/anbo.1997.0540

Doussan, C., A. Pierret, E. Garrigues, and L. Pagès. 2006. Water uptake by plant roots: II. Modelling of water transfer in the soil root-system with explicit account of flow within the root system—Comparison with experiments. Plant Soil 283:99–117. doi:10.1007/s11104-004-7904-z

Feddes, R.A., E. Bresler, and S.P. Neuman. 1974. Field test of a modified numerical model for water uptake by root systems. Water Resour. Res. 10:1199–1206. doi:10.1029/WR010i006p01199

Feddes, R.A., H. Hoff, M. Bruen, T. Dawson, P. de Rosnay, P. Dirmeyer, et al. 2001. Modeling root water uptake in hydrological and climate models. Bull. Am. Meteorol. Soc. 82:2797–2809. doi:10.1175/1520-0477(2001)082<2797:MRWUIH>2.3.CO;2

Feddes, R.A., P.J. Kowalik and H. Zaradny. 1978. Simulation of field water use and crop yield. PUDOC, Wageningen, the Netherlands.

Freundl, E., E. Steudle, and W. Hartung. 1998. Water uptake by roots of maize and sunflower affects the radial transport of abscisic acid and its concentration in the xylem. Planta 207:8–19. doi:10.1007/s004250050450

Garré, S., M. Javaux, J. Vanderborght, and H. Vereecken. 2011. Three-dimensional electrical resistivity tomography to monitor root zone water dynamics. Vadose Zone J. 10:412–424. doi:10.2136/vzj2010.0079

Garré, S., L. Pagès, E. Laloy, M. Javaux, J. Vanderborght, and H. Vereecken. 2012. Parameterizing a dynamic architectural model of the root system of spring barley from minirhizotron data. Vadose Zone J. 11(4). doi:10.2136/vzj2011.0179

Groh, J., J. Vanderborght, T. Pütz, and H. Vereecken. 2016. How to control the lysimeter bottom boundary to investigate the effect of climate change on soil processes? Vadose Zone J. 15(7). doi:10.2136/vzj2015.08.0113

Guderle, M., and A. Hildebrandt. 2015. Using measured soil water contents to estimate evapotranspiration and root water uptake profiles: A comparative study. Hydrol. Earth Syst. Sci. 19:409–425. doi:10.5194/hess-19-409-2015

Heinen, M. 2014. Compensation in root water uptake models combined with three-dimensional root length density distribution. Vadose Zone J. 13(2). doi:10.2136/vzj2013.08.0149

Hoffman, G.J. and M.Th. van Genuchten. 1983. Soil properties and efficient water use: Water management for salinity control. In: H.M. Taylor et al., editors, Limitations to efficient water use in crop production. ASA, CSSA, and SSSA, Madison, WI. p. 73–85.

Huang, B., R. Duncan, and R. Carrow. 1997. Drought-resistance mechanisms of seven warm-season turfgrasses under surface soil drying: II. Root aspects. Crop Sci. 37:1863–1869. doi:10.2135/cropsci1997.0011183X003700060033x

Huber, K., J. Vanderborght, M. Javaux, N. Schröder, I.C. Dodd, and H. Vereecken. 2014. Modelling the impact of heterogeneous root-zone water distribution on the regulation of transpiration by hormone transport and/or hydraulic pressures. Plant Soil 384:93–112. doi:10.1007/s11104-014-2188-4

Hupet, F., S. Lambot, R.A. Feddes, J.C. van Dam, and M. Vanclooster. 2003. Estimation of root water uptake parameters by inverse modeling with soil water content data. Water Resour. Res. 39:1312. doi:10.1029/2003WR002046

Hupet, F., S. Lambot, M. Javaux, and M. Vanclooster. 2002. On the identification of macroscopic root water uptake parameters from soil water content observations. Water Resour. Res. 38(12):1300. doi:10.1029/2002WR001556

Jarvis, N. 1989. A simple empirical model of root water uptake. J. Hydrol. 107:57–72. doi:10.1016/0022-1694(89)90050-4

Javaux, M., V. Couvreur, J. Vanderborght, and H. Vereecken. 2013. Root water uptake: From three-dimensional biophysical processes to macroscopic modeling approaches. Vadose Zone J. 12(4). doi:10.2136/vzj2013.02.0042

Javaux, M., T. Schröder, J. Vanderborght, and H. Vereecken. 2008. Use of a three-dimensional detailed modeling approach for predicting root water uptake. Vadose Zone J. 7:1079–1088. doi:10.2136/vzj2007.0115

Johnson, M., D. Tingey, D. Phillips, and M. Storm. 2001. Advancing fine root research with minirhizotrons. Environ. Exp. Bot. 45:263–289. doi:10.1016/S0098-8472(01)00077-6

Judd, L.A., B.E. Jackson, W.C. Fonteno, and J.-C. Domec. 2016. Measuring root hydraulic parameters of container-grown herbaceous and woody plants using the hydraulic conductance flow meter. HortScience 51:192–196.

Kropff, M.J., and H.H. van Laar. 1993. Modelling crop–weed interactions. CAB Int., Oxford, UK.

Krounbi, L., and N. Lazarovitch. 2011. Soil hydraulic properties affecting root water uptake. In: J. Gliński et al., editors, Encyclopedia of agrophysics. Springer, Dordrecht, the Netherlands. p. 748–754.

Kuhlmann, A., I. Neuweiler, S.E.A.T.M. van der Zee, and R. Helmig. 2012. Influence of soil structure and root water uptake strategy on unsaturated flow in heterogeneous media. Water Resour. Res. 48:W02534. doi:10.1029/2011WR010651

Kumar, R., V. Shankar and M.K. Jat. 2014. Evaluation of root water uptake models: A review. ISH J. Hydraul. Eng. 21:115–124. doi:10.1080/09715010.2014.981955

Lambot, S., M. Javaux, F. Hupet, and M. Vanclooster. 2002. A global multilevel coordinate search procedure for estimating the unsaturated soil hydraulic properties. Water Resour. Res. 38(11):1224. doi:10.1029/2001WR001224

Langensiepen, M., M. Kupisch, A. Graf, M. Schmidt, and F. Ewert. 2014. Improving the stem heat balance method for determining sap-flow in wheat. Agric. For. Meteorol. 186:34–42. doi:10.1016/j.agrformet.2013.11.007

Leffler, A.J., M.S. Peek, R.J. Ryel, C.Y. Ivans, and M.M. Caldwell. 2005. Hydraulic redistribution through the root systems of senesced plants. Ecology 86:633–642. doi:10.1890/04-0854

Li, K., R. De Jong, and J. Boisvert. 2001. An exponential root-water-uptake model with water stress compensation. J. Hydrol. 252:189–204. doi:10.1016/S0022-1694(01)00456-5

Lobet, G., V. Couvreur, F. Meunier, M. Javaux, and X. Draye. 2014. Plant water uptake in drying soils. Plant Physiol. 164:1619–1627. doi:10.1104/pp.113.233486

Lobet, G., and X. Draye. 2013. Novel scanning procedure enabling the vectorization of entire rhizotron-grown root systems. Plant Methods 9(1). doi:10.1186/1746-4811-9-1

Lynch, J.P. 2013. Steep, cheap and deep: An ideotype to optimize water and N acquisition by maize root systems. Ann. Bot. 112:347–357. doi:10.1093/aob/mcs293

Machado, R.M.A., M. do Rosário, and G. Oliveira. 2003. Comparison of tomato root distributions by minirhizotron and destructive sampling. In: J. Abe, editor, Roots: The dynamic interface between plants and the Earth. Dev. Plant Soil Sci. Ser. 101. Springer, Dordrecht, the Netherlands. p. 375–385. doi:10.1007/978-94-017-2923-9_36

MathWorks. 2015. MATLAB 2015b and statistics toolbox. The MathWorks, Natick, MA.

Miyamoto, N., E. Steudle, T. Hirasawa, and R. Lafitte. 2001. Hydraulic conductivity of rice roots. J. Exp. Bot. 52:1835–1846. doi:10.1093/jexbot/52.362.1835

Mo, X., and S. Liu. 2001. Simulating evapotranspiration and photosynthesis of winter wheat over the growing season. Agric. For. Meteorol. 109:203–222. doi:10.1016/S0168-1923(01)00266-0

Molz, F.J. 1981. Models of water transport in the soil–plant system: A review. Water Resour. Res. 17:1245–1260. doi:10.1029/WR017i005p01245

Mualem, Y. 1976. A new model for predicting the hydraulic conductivity of unsaturated porous media. Water Resour. Res. 12:513–522. doi:10.1029/WR012i003p00513

Musters, P., and W. Bouten. 1999. Assessing rooting depths of an Austrian pine stand by inverse modeling soil water content maps. Water Resour. Res. 35:3041–3048. doi:10.1029/1999WR900173

Musters, P., and W. Bouten. 2000. A method for identifying optimum strategies of measuring soil water contents for calibrating a root water uptake model. J. Hydrol. 227:273–286. doi:10.1016/S0022-1694(99)00187-0

Nelsen, C.E., G.R. Safir, and A.D. Hanson. 1978. Water potential in excised leaf tissue: Comparison of a commercial dew point hygrometer and a thermocouple psychrometer on soybean, wheat, and barley. Plant Physiol. 61:131–133. doi:10.1104/pp.61.1.131

Neumann, R.B., and Z.G. Cardon. 2012. The magnitude of hydraulic redistribution by plant roots: A review and synthesis of empirical and modeling studies. New Phytol. 194:337–352. doi:10.1111/j.1469-8137.2012.04088.x

Novák, V., K. Kňava, and J. Šimůnek. 2011. Determining the influence of stones on hydraulic conductivity of saturated soils using numerical method. Geoderma 161:177–181. doi:10.1016/j.geoderma.2010.12.016

O'Toole, J.C., and T.B. Moya. 1981. Water deficits and yield in upland rice. Field Crops Res. 4:247–259. doi:10.1016/0378-4290(81)90076-9

Oleson, K.W., G.-Y. Niu, Z.-L. Yang, D.M. Lawrence, P.E. Thornton, P.J. Lawrence, et al. 2008. Improvements to the community land model and their impact on the hydrological cycle. J. Geophys. Res. 113:G01021. doi:10.1029/2007JG000563

Pagès, L. 2011. Links between root developmental traits and foraging performance. Plant Cell Environ. 34:1749–1760. doi:10.1111/j.1365-3040.2011.02371.x

Pagès, L., G. Vercambre, J.-L. Drouet, F. Lecompte, C. Collet, and J. Le Bot. 2004. Root Typ: A generic model to depict and analyse the root system architecture. Plant Soil 258:103–119. doi:10.1023/B:PLSO.0000016540.47134.03

Pang, L., M.E. Close, J.P. Watt, and K.W. Vincent. 2000. Simulation of picloram, atrazine, and simazine leaching through two New Zealand soils and into groundwater using HYDRUS-2D. J. Contam. Hydrol. 44:19–46. doi:10.1016/S0169-7722(00)00091-7

Pang, X., and J. Letey. 1998. Development and evaluation of ENVIRO-GRO, an integrated water, salinity, and nitrogen model. Soil Sci. Soc. Am. J. 62:1418–1427. doi:10.2136/sssaj1998.03615995006200050039x

Pierret, A., C. Doussan, and L. Pages. 2006. Spatio-temporal variations in axial conductance of primary and first-order lateral roots of a maize crop as predicted by a model of the hydraulic architecture of root systems. Plant Soil 282:117–126. doi:10.1007/s11104-005-5373-7

Rewald, B., and J.E. Ephrath. 2012. Minirhizotron techniques. In: A. Eschel and T. Beekmann, editors, Plant roots: The hidden half. 4th ed. CRC Press, Boca Raton, FL. doi:10.1201/b14550-50

Richards, J.H., and M.M. Caldwell. 1987. Hydraulic lift: Substantial nocturnal water transport between soil layers by *Artemisia tridentata* roots. Oecologia 73:486–489. doi:10.1007/BF00379405

Rothfuss, Y., and M. Javaux. 2016. Isotopic approaches to quantifying root water uptake and redistribution: A review and comparison of methods. Biogeosciences 14:2199–2224. doi:10.5194/bg-14-2199-2017

Schaap, M.G., and F.J. Leij. 2000. Improved prediction of unsaturated hydraulic conductivity with the Mualem–van Genuchten model. Soil Sci. Soc. Am. J. 64:843–851. doi:10.2136/sssaj2000.643843x

Shen, J., W.D. Batchelor, J.W. Jones, J.T. Ritchie, R.S. Kanwar, and C.W. Mize. 1998. Incorporation of a subsurface tile drainage component into a soybean growth model. Trans. ASAE 41:1305–1313. doi:10.13031/2013.17303

Shen, Y., Y. Zhang, and S. Li. 2011. Nutrient effects on diurnal variation and magnitude of hydraulic lift in winter wheat. Agric. Water Manage. 98:1589–1594. doi:10.1016/j.agwat.2011.05.012

Shimshi, D. 1979. Leaf permeability as an index of water relations, CO_2 uptake and yield of irrigated wheat. Irrig. Sci. 1:107–117. doi:10.1007/BF00263094

Šimůnek, J., and J.W. Hopmans. 2009. Modeling compensated root water and nutrient uptake. Ecol. Modell. 220:505–521. doi:10.1016/j.ecolmodel.2008.11.004

Šimůnek, J., M. Sejna, H. Saito, M. Sakai, and M.Th. van Genuchten. 2013. The HYDRUS-1D software package for simulating the movement of water, heat, and multiple solutes in variably saturated media, Version 4.16. HYDRUS Softw. Ser. 3. Dep. of Environ. Sci., Univ. of California, Riverside.

Šimůnek, J., and D.L. Suarez. 1993. Modeling of carbon dioxide transport and production in soil: 1. Model development. Water Resour. Res. 29:487–497. doi:10.1029/92WR02225

Šimůnek, J., O. Wendroth, and M.Th. van Genuchten. 1998. Parameter estimation analysis of the evaporation method for determining soil hydraulic properties. Soil Sci. Soc. Am. J. 62:894–905. doi:10.2136/sssaj1998.03615995006200040007x

Skaggs, T.H., M.Th. van Genuchten, P.J. Shouse, and J.A. Poss. 2006. Macroscopic approaches to root water uptake as a function of water and salinity stress. Agric. Water Manage. 86:140–149. doi:10.1016/j.agwat.2006.06.005

Smucker, A.J.M., J.C. Ferguson, W.P. DeBruyn, R.K. Belford, and J.T. Ritchie. 1987. Image analysis of video-recorded plant root systems. In: H.M. Taylor, editor, Minirhizotron observation tubes: Methods and applications for measuring rhizosphere dynamics. ASA Spec. Publ. 50. ASA, CSSA, and SSSA, Madison, WI. p. 67–80. doi:10.2134/asaspecpub50.c6

Somma, F., J.W. Hopmans, and V. Clausnitzer. 1998. Transient three-dimensional modeling of soil water and solute transport with simultaneous root growth, root water and nutrient uptake. Plant Soil 202:281–293. doi:10.1023/A:1004378602378

Steele, S.J., S.T. Gower, J.G. Vogel, and J.M. Norman. 1997. Root mass, net primary production and turnover in aspen, jack pine and black spruce forests in Saskatchewan and Manitoba, Canada. Tree Physiol. 17:577–587. doi:10.1093/treephys/17.8-9.577

Steudle, E., R. Oren, and E.-D. Schulze. 1987. Water transport in maize roots: Measurement of hydraulic conductivity, solute permeability, and of reflection coefficients of excised roots using the root pressure probe. Plant Physiol. 84:1220–1232. doi:10.1104/pp.84.4.1220

Steudle, E., and C.A. Peterson. 1998. How does water get through roots? J. Exp. Bot. 49:775–788. 10.1093/jexbot/49.322.775

Tardieu, F., and T. Simonneau. 1998. Variability among species of stomatal control under fluctuating soil water status and evaporative demand: Modelling isohydric and anisohydric behaviours. J. Exp. Bot. 49:419–432. doi:10.1093/jxb/49.Special_Issue.419

Thoma, M.J., W. Barrash, M. Cardiff, J. Bradford, and J. Mead. 2014. Estimating unsaturated hydraulic functions for coarse sediment from a field-scale infiltration experiment. Vadose Zone J. 13(3). doi:10.2136/vzj2013.05.0096

Toorman, A.F., P.J. Wierenga, and R.G. Hills. 1992. Parameter estimation of hydraulic properties from one-step outflow data. Water Resour. Res. 28:3021–3028. doi:10.1029/92WR01272

Tyree, M.T., S. Patiño, J. Bennink, and J. Alexander. 1995. Dynamic measurements of roots hydraulic conductance using a high-pressure flowmeter in the laboratory and field. J. Exp. Bot. 46:83–94. doi:10.1093/jxb/46.1.83

Upchurch, D.R. 1987. Conversion of minirhizotron–root intersections to root length density. In: H.M. Taylor, editor, Minirhizotron observation tubes: Methods and applications for measuring rhizosphere dynamics. ASA Spec. Publ. 50. ASA, Madison, WI. p. 51–65. doi:10.2134/asaspecpub50.c5

Vamerali, T., M. Bandiera, and G. Mosca. 2012. Minirhizotrons in modern root studies. In: S. Mancuso, editor, Measuring roots: An updated approach. Springer, Heidelberg, Germany. p. 341-361. doi:10.1007/978-3-642-22067-8_17

van den Honert, T.H. 1948. Water transport in plants as a catenary process. Discuss. Faraday Soc. 3:146–153. doi:10.1039/df9480300146

Vanderborght, J., A. Graf, C. Steenpass, B. Scharnagl, N. Prolingheuer, M. Herbst, et al. 2010. Within-field variability of bare soil evaporation derived from eddy covariance measurements. Vadose Zone J. 9:943–954. doi:10.2136/vzj2009.0159

Vandoorne, B., L. Beff, S. Lutts, and M. Javaux. 2012. Root water uptake dynamics of *Cichorium intybus* var. *sativum* under water-limited conditions. Vadose Zone J. 11(3). doi:10.2136/vzj2012.0005

van Genuchten, M.Th. 1980. A closed-form equation for predicting the hydraulic conductivity of unsaturated soils. Soil Sci. Soc. Am. J. 44:892–898. doi:10.2136/sssaj1980.03615995004400050002x

Vansteenkiste, J., J. Van Loon, S. Garré, L. Pagès, E. Schrevens, and J. Diels. 2014. Estimating the parameters of a 3-D root distribution function from root observations with the trench profile method: Case study with simulated and field-observed root data. Plant Soil 375:75–88. doi:10.1007/s11104-013-1942-3

Vereecken, H., J.A. Huisman, H.J.H. Franssen, N. Brüggemann, H.R. Bogena, S. Kollet, et al. 2015. Soil hydrology: Recent methodological advances, challenges, and perspectives. Water Resour. Res. 51:2616–2633. doi:10.1002/2014WR016852

Vereecken, H., A. Schnepf, J.W. Hopmans, M. Javaux, D. Or, T. Roose, et al. 2016. Modeling soil processes: Review, key challenges, and new perspectives. Vadose Zone J. 15(5). doi:10.2136/vzj2015.09.0131

Vereecken, H., M. Weynants, M. Javaux, Y. Pachepsky, M. Schaap, and M.Th. Genuchten. 2010. Using pedotransfer functions to estimate the van Genuchten–Mualem soil hydraulic properties: A review. Vadose Zone J. 9:795–820. doi:10.2136/vzj2010.0045

Volkmar, K. 1993. A comparison of minirhizotron techniques for estimating root length density in soils of different bulk densities. Plant Soil 157:239–245. doi:10.1007/BF00011052

Vrugt, J.A., J.W. Hopmans, and J. Šimůnek. 2001a. Calibration of a two-dimensional root water uptake model. Soil Sci. Soc. Am. J. 65:1027–1037. doi:10.2136/sssaj2001.6541027x

Vrugt, J.A., and C.J.F. Ter Braak. 2011. DREAM$_{(D)}$: An adaptive Markov chain Monte Carlo simulation algorithm to solve discrete, noncontinuous, and combinatorial posterior parameter estimation problems. Hydrol. Earth Syst. Sci. 15:3701–3713. doi:10.5194/hess-15-3701-2011

Vrugt, J.A. , M.T. van Wijk, J.W. Hopmans, and J. Šimůnek. 2001b. One-, two-, and three-dimensional root water uptake functions for transient modeling. Water Resour. Res. 37:2457–2470. doi:10.1029/2000WR000027

Weihermüller, L., J.A. Huisman, N. Hermes, S. Pickel, and H. Vereecken. 2013. A new TDR multiplexing system for reliable electrical conductivity and soil water content measurements. Vadose Zone J. 12(2). doi:10.2136/vzj2012.0194

Wells, C., and S. Birchfield. 2009. Rootfly: Software for minirhizotron image analysis. Clemson Univ., Kingstree, SC.

Wesseling, J. 1991. Meerjarige simulaties van grondwateronttrekking voor verschillende bodemprofielen, grondwatertrappen en gewassen met het model SWATRE. SC-DLO Rep. 152. DLO Winand Staring Ctr., Wageningen, the Netherlands.

Wesseling, J., and T. Brandyk. 1985. Introduction of the occurrence of high groundwater levels and surface water storage in computer program SWATRE. ICW, Wageningen, the Netherlands.

Wesseling, J., J. Elbers, P. Kabat, and B. van den Broek. 1991. SWATRE: Instructions for input. Internal note. Winand Staring Ctr., Wageningen, the Netherlands.

Willmott, C.J., S.G. Ackleson, R.E. Davis, J.J. Feddema, K.M. Klink, D.R. Legates, et al. 1985. Statistics for the evaluation and comparison of models. J. Geophys. Res. 90(C5):8995–9005. doi:10.1029/JC090iC05p08995.

Wöhling, T., S. Gayler, E. Priesack, J. Ingwersen, H.D. Wizemann, P. Högy, et al. 2013. Multiresponse, multiobjective calibration as a diagnostic tool to compare accuracy and structural limitations of five coupled soil–plant models and CLM3.5. Water Resour. Res. 49:8200–8221. doi:10.1002/2013WR014536

Wu, J., R. Zhang, and S. Gui. 1999. Modeling soil water movement with water uptake by roots. Plant Soil 215:7–17. doi:10.1023/A:1004702807951

Yang, D., T. Zhang, K. Zhang, D.J. Greenwood, J.P. Hammond, and P.J. White. 2009. An easily implemented agro-hydrological procedure with dynamic root simulation for water transfer in the crop–soil system: Validation and application. J. Hydrol. 370:177–190. doi:10.1016/j.jhydrol.2009.03.005

Yates, S.R., M.Th. van Genuchten, A.W. Warrick, and F.J. Leij. 1992. Analysis of measured, predicted, and estimated hydraulic conductivity using the RETC computer program. Soil Sci. Soc. Am. J. 56:347–354. doi:10.2136/sssaj1992.03615995005600020003x

Zegada-Lizarazu, W., and M. Iijima. 2004. Hydrogen stable isotope analysis of water acquisition ability of deep roots and hydraulic lift in sixteen food crop species. Plant Prod. Sci. 7:427–434. doi:10.1626/pps.7.427